# Author response to anonymous referee #1 on "An intercomparison of $CH_3O_2$ measurements by Fluorescence Assay by Gas Expansion and Cavity Ring–Down Spectroscopy within HIRAC (Highly Instrumented Reactor for Atmospheric Chemistry)" by L. Onel et al.

**Note:** The authors' changes of the text in response to the referees' comments refer to the numbers of the lines and the pages of the manuscript before revision.

**General comments**

*Regarding the calibration of the FAGE, it was surprising that the water vapour photolysis method was not used at all conditions studied. This instrument has been deployed on aircraft, so sensitivities for OH and HO2 were surely determined as a function of sample pressure.*

The HIRAC FAGE instrument has not been deployed on an aircraft, although the Leeds aircraft FAGE instrument (Commane et al., 2010) does have fluorescence cells of a similar design to those used in HIRAC for this $CH_3O_2$ work. The sensitivity towards OH and $HO_2$ as a function of pressure of the fluorescence cell was determined for the HIRAC FAGE instrument (Winiberg et al., 2015), and also for the aircraft instrument (Commane et al., 2010). However, in both cases the sample pressure was not changed, rather the pressure in the fluorescence cell was altered by using different sized pinholes to reflect the same pressure as whilst sampling from reduced pressure (either at different altitudes on the aircraft or from HIRAC operating at reduced pressure). For the aircraft instrument there was very little dependence of the sensitivity with cell pressure for the range of altitudes encountered for both OH and $HO_2$ (Commane et al., 2010). For HIRAC, a small increase in the sensitivity for OH was seen, and a larger change for $HO_2$ was seen over the range of cell pressures used (Winiberg et al., 2015), although the experiments were performed at a range of pulse repetition frequencies, and different pumps were used for the aircraft and HIRAC pressure dependencies. This approach, which assumes there is no change in any losses at the pinhole across a changing pressure differential, was validated by another group for an aircraft instrument using different materials for the pinhole (Faloona et al., 2004). In HIRAC, we validated the approach by employing the decay of a hydrocarbon in HIRAC at different pressures in the presence of OH which was measured using FAGE, or that of $HO_2$ by its kinetic decay followed production via the photolysis of HCHO at different pressures, and obtained the same result as using the water vapour calibration method.

References

Commane, R., Floquet, C. F. A., Ingham, T., Stone, D., Evans, M. J., and Heard, D. E.: Observations of OH and $HO_2$ radicals over West Africa, *Atmos. Chem. Phys*., 10, 8783–8801, 2010.

Winiberg, F. A. F., Smith, S. C., Bejan, I., Brumby, C. A., Ingham, T., Malkin, T. L., Orr, S. C., Heard, D. E., and Seakins, P. W.: Pressuredependent calibration of the OH and HO2 channels of a FAGE HOx instrument using the Highly Instrumented Reactor for Atmospheric Chemistry (HIRAC), *Atmos. Meas. Tech*., 8, 523-540, 2015.

Faloona, I. C., Tan, D., Lesher, R. L., Hazen, N. L., Frame, C. L., Simpas, J. B., Harder, H., Martinez, M., Di Carlo, P., Ren, X. R., and Brune, W. H.: A laser-induced fluorescence instrument for detecting tropospheric OH and HO2: Characteristics and calibration, *J. Atmos. Chem*., 47, 139–167, 2004

*It is straightforward to make use of this calibration procedure at reduced pressures for methylperoxy radicals. The paper would be greatly improved by performing such calibrations for the two other chamber conditions.*

In this paper, rather than validating the water vapour method for the calibration of $CH_3O_2$ sensitivity as a function of pressure (using a known OH which is converted to $CH_3O_2$, followed by conversion to $CH_3O$ by NO, and the $CH_3O$ formed detected (Onel et al. 2017b in the list of references of the manuscript), the main aim was to compare two distinct techniques (FAGE and CRDS) for a range of sampling conditions. Also, it is felt that because the sample pressure cannot be reduced in these experiments during the calibration (rather a change in pinhole is used or a change in pumping capacity is used to change the cell pressure, which would change the residence time from sampling to the laser-excitation axis), that additional uncertainties would arise in determining the sensitivity of

FAGE to $CH_3O_2$ as a function of pressure using the water vapour calibration method, so it was used at atmospheric pressure to calibrate $CH_3O_2$.

*On the other hand, since there is a systematic difference between the two methods of calibrations at 1000 torr, and that the authors favor the water vapour photolysis method (indicating that perhaps the rate coefficient for methylperoxy radical decay, kobs, should be reduced by 25-30%), it appears to this reviewer that perhaps the FAGE calibration factors for the 80 mbar and 100 mbar should be scaled by the ratio of the calibration factors for the two methods performed at 1000 mbar. If the rate coefficient is indeed in error, the CRDS calibrations should also be adjusted by the same factor. As stated in the paper, though, if both instruments rely on methylperoxy radical decay for their calibration, then the accuracy of the value for kobs does not matter, if the same value is used for both.*

The referee is correct, the same value is used for both and so the accuracy of the value for $k_{obs}$ does not matter. The kinetic method used for the determination of the $CH_3O_2$ absorption cross-section, $\sigma_{CH3O2}$ relies on the value for the rate coefficient of the $CH_3O_2$ self-reaction. However, as the previous studies at a range of pressures typically used the $CH_3O_2$ kinetic decay to determine $\sigma_{CH3O2}$, the kinetic method of calibration was chosen in this work for comparisons of the value of $\sigma_{CH3O2}$ obtained in this work with the values for $\sigma_{CH3O2}$ reported previously.

The water vapour photolysis method of calibration is a well-established method for FAGE calibration (*vide supra*), routinely used in calibrations at atmospheric pressure. Therefore, both methods of FAGE calibration, the water vapour photolysis method and the kinetic method, were employed in this work at atmospheric pressure. As noted by the referee, a systematic 25–30% discrepancy was found between the FAGE sensitivities factors, $C_{CH3O2}$ obtained by the two methods at atmospheric pressure (this work and Onel et al. 2017b in the list of references of the manuscript). As the water vapour photolysis method is known to be an accurate and reliable method of calibration, the discrepancy at atmospheric pressure would seem to indicate that the value of $k_{obs}$ (Atkinson et al. 2006) is overestimated by 25–30%. This is already discussed in detail in the main text (see lines 24 – 30, page 15 and lines 19 – 30, page 17).

*It was also not obvious from the paper what kobs referred to, so suggest adding some text to indicate that it refers to the effective rate coefficient for second order methylperoxy radical decay that includes contributions from methylperoxy radicals reacting with HO2, which is produced from R5b followed by the rapid reaction of methoxy radicals with oxygen. It is possible that this is what lines 31-34 on page 6 were trying to say, but it was not clear to this reviewer. Suggest rewriting this text and/or adding more information. Note that without radical wall loss, kobs = k5a+2k5b. It would be useful to add discussion on the impact of HO2 wall loss on kobs both in the present experiments, and in those used by IUPAC to arrive at their kinetic recommendations.*

Following the suggestions of the referees the paragraph in the MS corresponding to lines 26-33 on page 6 was changed and now includes both the expression used for the observed rate coefficient in line with IUPAC recommendation: $k_{obs} = k_5(1 + r_{5b})$, where $r_{5b}$ is the branching ratio for the channel R5b, and the rationale behind this expression (see also the response to the other comment regarding line 26 on page 6, see below):

"As each $HO_2$ radical consumes rapidly one $CH_3O_2$ species on the time scale of the reaction R5, the $CH_3O_2$ decay is described by second order kinetics (Sander and Watson, 1980); (Sander and Watson, 1981;McAdam et al., 1987;Kurylo and Wallington, 1987;Jenkin et al., 1988;Simon et al., 1990), with $k_{obs} = k_5(1 + r_{5b})$, where $r_{5b}$ is the branching ratio for the channel R5b. By using the IUPAC recommendations (Atkinson et al., 2006): $k_5 = (3.5 \pm 1.0) \times 10^{-13}$ molecule$^{-1}$ cm$^3$ s$^{-1}$ and $r_{5b} = 0.37 \pm 0.06$, a value of $4.8 \times 10^{-13}$ molecule$^{-1}$ cm$^3$ s$^{-1}$ is obtained for $k_{obs}$. Modelling of the decay process with a variety of $CH_3O_2$ and $HO_2$ concentrations after the lamps were switched off and following the establishment of steady state conditions showed that Eq. (3) was valid within experimental error. With $k_5 = 3.5 \times 10^{-13}$ molecule$^{-1}$ cm$^3$ s$^{-1}$ (Atkinson et al., 2006), a faster observed rate constant (defined by Eq. (3)) was obtained from the model with a value, $4.9 \times 10^{-13}$ molecule$^{-1}$ cm$^3$ s$^{-1}$ consistent with that recommended by IUPAC, $(4.8 \pm 0.6) \times 10^{-13}$ molecule$^{-1}$ cm$^3$ s$^{-1}$ ($1\sigma$ uncertainty; Atkinson et al., 2006). Substituting …"

Details of the experiments which investigated the potential impact of the $HO_2$ wall loss on the value of $k_{obs}$ are included in the response to the comment regarding line 12 on page 7 and described in a paragraph added above Fig. 1, and included in the same response (*vide infra*).

*Regarding the three conditions for the intercomparison: why were these selected? Would it have made sense to perform experiments in air at a variety of pressures (say five) between 100 and 1000 mbar? It is not apparent why helium/oxygen mixtures were used. Suggest adding some more discussion of the reasoning for the selection of chamber conditions for the intercomparisons.*

The pressure of 1000 mbar of synthetic air was chosen to perform measurements under atmospheric conditions. To the best of our knowledge this is the first study of the $CH_3O_2$ absorption feature centred around 7488 $cm^{-1}$ at a relatively high pressure. The previous studies were performed at reduced pressures, in the range ~30 – 200 mbar (see the introduction of the main text). In order to enable comparison with the reported studies of the $CH_3O_2$ spectrum and also test the performance of both instruments (FAGE and CRDS) at reduced pressure part of the experiments were performed at 100 mbar of synthetic air. The pressure of 80 mbar $He/O_2$ mixture was chosen as the most recent reported $CH_3O_2$ absorption spectrum (Faragó et al. 2013) was obtained at reduced pressures (70 and 133 mbar) of $He/O_2$ mixtures. The text describes all the conditions used previously in the studies of the $CH_3O_2$ absorption spectrum, so already provides some reasoning for why these conditions were chosen.

*Clearly, analytical techniques for methylperoxy radicals are going to be useful in application to reactions of these radicals, such as R5 and R12. This paper states that studies of R5 kinetics will be reported in another paper. The authors may wish to consider publishing the other paper first, since such results could have direct bearing on the results of this paper.*

The purpose of the present study is to provide a validation of the LIF method for $CH_3O_2$ measurements. As mentioned by the referee, even if the value of $\sigma_{CH3O2}$ does rely on the kinetics of the $CH_3O_2$ self-reaction, the $\sigma_{CH3O2}$ value obtained does not affect the results of the FAGE – CRDS intercomparison (as the same value for $k_{obs}$ is used for both) and, hence the validation of the FAGE method. We would like to publish the present results first, which provide a validation of the newly LIF method for $CH_3O_2$ before reporting kinetic studies of $CH_3O_2$ reactions employing the method. A detailed paper describing extensive studies of kinetics of the $CH_3O_2$ self-reaction over a range of temperatures is in preparation. This publication will enable to scale the value of $\sigma_{CH3O2}$ based on any change value of $k_{obs}$ for the $CH_3O_2$ self-reaction, as noted by the referee in the general comments (see above). The current paper is written to be consistent with the detailed kinetics paper to follow. We also mention that referee 2 notes this comment by referee 1, but did not feel that the kinetics paper needed to be published first.

**Specific comments**

*Page 4, line 24, 31-33. Very high concentrations of chlorine, methane and acetone were used in these experiments. Have you verified that these high amounts do not affect the performance of the instruments through interferences or artifacts? If so, suggest adding a discussion of the tests that were performed.*

We respond on this comment first for the CRDS instrument, then for the FAGE instrument.

**CRDS instrument**

The concentrations of the reagents were chosen to generate a range of $CH_3O_2$ concentrations above the detection limit of CRDS at each pressure (Table 2, page 14 in the main manuscript). The molecular chlorine delivery did not result in a change in the ring-down time. However, the methane and acetone delivery led to a decrease in the ring down time due to their absorbance in the range ~7486–7491 $cm^{-1}$ used in the CRDS measurements. The absorption coefficient of acetone in a typical concentration of ~$9 \times 10^{14}$ molecule $cm^{-3}$ was measured in the absence of $CH_3O_2$ (before to turn the HIRAC lamps on to generate $CH_3O_2$) to obtain a value of ~$8 \times 10^{-9}$ $cm^{-1}$ at 7487.98 $cm^{-1}$. Similar measurements, in the absence $CH_3O_2$ were performed to determine the $CH_4$ absorption coefficient, $\alpha_{CH4}$. For the typical concentrations of $CH_4$, in the range of (1.2–2.5) $\times 10^{16}$ molecule $cm^{-3}$, $\alpha_{CH4,\ 7487.98\ cm\text{-}1} \approx (0.7 – 1.4) \times 10^{-8}$ $cm^{-1}$. The absorption of acetone and methane in the background of the CRDS measurements of $CH_3O_2$ was taken into account in the determination of the $[CH_3O_2]_{CRDS}$. We have modified the wording in the MS as described in the paragraph below, added after line 10, page 10:

"The molecular chlorine delivery did not result in a change in the measured ring-down time. However, he delivery of the methane and acetone reagents led to a decrease in the ring-down time indicating that, in the concentrations delivered to the chamber, methane and acetone absorbed in the wavenumber range used in the present work, ~7486–7491 $cm^{-1}$. An absorption coefficient of ~$8 \times 10^{-9}$ $cm^{-1}$ was measured for [acetone] ≈ $9 \times 10^{14}$ molecule $cm^{-3}$ at the

typical measurement point of 7487.98 $cm^{-1}$ (*vide infra*). An absorption coefficient in the range (0.7–1.4) × $10^{-8}$ $cm^{-1}$ was determined at 7487.98 $cm^{-1}$ for $CH_4$ in typical concentrations in the FAGE–CRDS intercomparison experiments in the range (1.2–2.5) × $10^{16}$ molecule $cm^{-3}$. The background ring-down time $\tau_0$ (Eq. 7) contained the contributions of the reagents, methane or acetone, and was monitored regularly during the experiments by turning off the chamber lamps (*vide supra*)."

**FAGE instrument**

The concentrations of the reagents were a few orders of magnitude smaller in the fluorescence detection cell than in the HIRAC chamber as the gas mixture was sampled into the FAGE instrument through a 1.0 mm diameter pinhole nozzle resulting in the pressure in the FAGE detection cell being a few orders of magnitude lower than the pressure in HIRAC. The concentrations of the reagents were changed with no discernible change in the FAGE sensitivity factor – this is now mentioned in the text, see below.

The lines 39- 40, page 4 in Sect 2.2 were changed to …:

"…The interior of the tube is held at a low pressure (3.3 mbar for a HIRAC pressure, $p_{HIRAC}$ of 1000 mbar of synthetic air and 0.9 mbar for $p_{HIRAC}$ = 100 mbar synthetic air and $p_{HIRAC}$ = 80 mbar mixture of $He:O_2$ = 3:1) and..."

The investigations described below showed that there was no effect of the concentrations of the reagents ($Cl_2$, methane and acetone) on the sensitivity factor of FAGE.

The following text was added after line 17, page 8 in the section 2.2.2:

"As the pressure in the FAGE detection cell was 2-3 orders of magnitude lower than the corresponding pressure in HIRAC (*vide supra* in Sect. 2.2) the concentrations of the reagents ($Cl_2$, methane and acetone) were also 2-3 orders of magnitude lower in the fluorescence cells than the reagent concentrations in HIRAC. However, a potential effect of the reagents ($Cl_2$, methane and acetone) on the FAGE sensitivity factor in the HIRAC experiments was investigated. Two different concentrations of $CH_4$ were used in the kinetic method for FAGE calibration at 80 mbar of He + $O_2$ in HIRAC to find practically the same sensitivity factor: (3.80 ± 0.50) × $10^{-9}$ counts $cm^3$ $molecule^{-1}$ $s^{-1}$ $mW^{-1}$ for 2.5 × $10^{16}$ molecule $cm^{-3}$ $CH_4$ (2.8 × $10^{14}$ molecule $cm^{-3}$ in the fluorescence cell) and (3.86 ± 0.50) × $10^{-9}$ counts $cm^3$ $molecule^{-1}$ $s^{-1}$ $mW^{-1}$ for 2.5 × $10^{17}$ molecule $cm^{-3}$ $CH_4$ (2.8 × $10^{15}$ molecule $cm^{-3}$ in the fluorescence cell).

As shown in Fig. S1 in the Supplement there is a good agreement between the laser excitation scans of $CH_3O$ obtained from the $CH_3O_2$ generated in HIRAC using the two methods: acetone photolysis and $Cl_2$ photolysis in the presence of $CH_4$ and $O_2$. In addition, a good agreement has been previously found between the laser excitation spectra of $CH_3O$ generated using the reaction of $CH_4$ with OH (generated by the 254 nm photolysis of water) in the presence of $O_2$ and directly, through the 254 nm photolysis of $CH_3OH$. Therefore, no effect of the used reagents on the laser excitation spectrum of $CH_3O$ was found."

*Page 4, line 38 to page 5, line5. Suggest giving the transit times in addition to the distances in describing the sample moving through the FAGE.*

Line 41, page 4: The value given for the flow rate of the gas sampled through the FAGE pinhole was corrected:

"…on one end of the tube at a rate of ~3 SLM."

A sentence was added in the line 4 at page 5:

" … $CH_3O_2$ measurements detailed here. The $CH_3O_2$ radicals sampled through the FAGE pinhole at 1000 mbar in HIRAC reached the detection region in about 85 ms."

*Page 5, line 11-12. Suggest giving units for $C_{CH3O2}$ and $S_{CH3O2}$ factors.*

The units were included in the text.

*Page 6, equations 3, 4, and 5. Suggest using Δt instead of t in these equations.*

*t* was changed to Δ*t* in the equations.

*Page 6, line 26. Suggest rewording "…does not stop the decay analysis…" and page 6, lines 30-34. Suggest rewording (mentioned earlier) this discussion.*

Lines 26-33 on page 6 were reworded:

"As each $HO_2$ radical consumes rapidly one $CH_3O_2$ species on the time scale of the reaction R5, the $CH_3O_2$ decay is described by second order kinetics (Sander and Watson, 1980); (Sander and Watson, 1981; McAdam et al., 1987; Kurylo and Wallington, 1987; Jenkin et al., 1988; Simon et al., 1990), with $k_{obs} = k_5(1 + r_{5b})$, where $r_{5b}$ is the branching ratio for the channel R5b. By using the IUPAC recommendations (Atkinson et al., 2006): $k_5 = (3.5 \pm 1.0) \times 10^{-13}$ molecule$^{-1}$ cm$^3$ s$^{-1}$ and $r_{5b} = 0.37 \pm 0.06$, a value of $4.8 \times 10^{-13}$ molecule$^{-1}$ cm$^3$ s$^{-1}$ is obtained for $k_{obs}$.

Modelling of the decay process with a variety of $CH_3O_2$ and $HO_2$ concentrations after the lamps were switched off and following the establishment of steady state conditions showed that Eq. (3) was valid within experimental error. With $k_5 = 3.5 \times 10^{-13}$ molecule$^{-1}$ cm$^3$ s$^{-1}$ (Atkinson et al., 2006), a faster observed rate constant (defined by Eq. (3)) was obtained from the model with a value, $4.9 \times 10^{-13}$ molecule$^{-1}$ cm$^3$ s$^{-1}$ consistent with that recommended by IUPAC, $(4.8 \pm 0.6) \times 10^{-13}$ molecule$^{-1}$ cm$^3$ s$^{-1}$ ($1\sigma$ uncertainty; Atkinson et al., 2006). Substituting …"

*Page 7, lines 1 and 3. Suggest adding discussion of the fitting procedure used in this paper, both for the radical signal decays and the instrument comparisons.*

The fitting algorithm was included in line 2, page 7: "which is then used to fit to the experimental data with $k_{obs}$ fixed to the value recommended by IUPAC for 298 K, $4.8 \times 10^{-13}$ molecule$^{-1}$ cm$^3$ s$^{-1}$, using the Levenberg-Marquardt algorithm."

Lines 20-22, page 7 (caption of figure 1): The value given for $C_{CH3O2}$ was corrected and the used fitting algorithm was included: "The data were fitted to Eq. (5) (excluding the wall loss rate, $k_{loss}$; red line) and Eq. (6) (including $k_{loss}$; blue dashed line) using the Levenberg-Marquardt algorithm. The obtained value for the sensitivity factor was the same by both fits: $C_{CH3O2} = (1.17 \pm 0.04) \times 10^{-9}$ counts cm$^3$ molecule$^{-1}$ s$^{-1}$ mW$^{-1}$."

The discussion of the fitting procedure used in the FAGE-CRDS correlation plots was added to the text (*vide infra*).

*Page 7, line 12. It is stated that "…wall losses are very small and can be neglected." Suggest adding an upper limit for the wall loss of CH3O2 and for HO2 (since this bears on the decay of CH3O2).*

The upper limit for the wall loss rate coefficient of $CH_3O_2$ was added (lines 11-12 on page7): "… the small values extracted for $k_{loss}$ (upper limit of ~ $1 \times 10^{-5}$ s$^{-1}$) fitting Eq. (6) demonstrates that wall losses can be neglected."

A paragraph regarding investigations into a potential impact of the wall loss of $HO_2$ on the analysis was added above figure 1:

"Modelling the $CH_3O_2$ decays including a wall loss for $HO_2$ in the range of measured values 0.03 – 0.09 s$^{-1}$ (Onel et al. 2017a in the MS), showed an minor impact of the wall loss of $HO_2$ on $k_{obs}$, i.e. $k_{obs}$ within 98 – 95 % agreement with the IUPAC preferred value, $(4.8 \pm 0.6) \times 10^{-13}$ molecule$^{-1}$ cm$^3$ s$^{-1}$ ($1\sigma$ uncertainty; Atkinson et al., 2006)."

*Page 7, line 21-22. It appears that the exponent for the sensitivity should be "-9" rather than "-10" as shown.*

The power was changed to "-9".

*Page 8, line 9. Suggest "…S2 and S3, respectively."*

A comma was added after S3.

*Page 8, line 30. Does the large amount of ozone affect the instrument performance?*

No effect of $O_3$ on the instrument was encountered. Note that due to the lower pressure in the FAGE detection cell (3.3 mbar) compared to the pressure in the chamber (1000 mbar) in these experiments $[O_3]_{FAGE} = 8.3 \times 10^{10}$ molecule $cm^{-3}$ for $[O_3]_{HIRAC} = 2.5 \times 10^{13}$ molecule $cm^{-3}$.

*Page 10, line 14. Is it not possible to keep the radical concentration stable for more than 5 minutes? Perhaps this sentence needs rewording.*

The result was revised and the time was changed from 5 min to 10 min.

*Page 10, line 35. Suggest rewording "…potential small difference in wavelength compared to λ in the spectrum…". The meaning is not clear as written.*

The below text was included in line 18, page 10 to respond to the referee 2 comment:

*Why the authors measure absorption at 7488 cm-1 when Fittschen(2019) report σ (v) at 7489 cm-1?*

"…was determined (Sect. 3.2). The absorption coefficient of $CH_4$ was about 7 times lower at 7487.98 cm-1 than at 7489.16 $cm^{-1}$, i.e. at the peak of the $CH_3O_2$ spectral feature where Fittschen (2019) reported $\sigma_{CH3O2}$. Therefore, 7487.98 $cm^{-1}$ (rounded to 7488 $cm^{-1}$ henceforth) was chosen as the measurement point instead of the value of 7489.16 $cm^{-1}$ used by Fittschen (2019). Each datum point in Fig. 3…"

Note that above the word "data" was changed to "datum".

Due to the difference in the resolution of the two $CH_3O_2$ spectra – the spectrum obtained in this work and the spectrum reported by Faragó et al. (2013) – it is difficult to realise if there are any slight shifts of the spectrum found by Faragó et al. (2013) relative to the spectrum reported in this study. Therefore the words "which did not allow for a high resolution" and " potential small difference in wavelength compared to λ in the spectrum" on line 34-35, page 10 were removed and therefore, the lines 33 – 35, page 10 are changed to:

"The peaks at the top of the spectral feature reported by Faragó et al. (2013) are not reproduced in this work owing to the method of generating the spectrum (Sect. 2.3). Previously Pushkarsky et al. (2000)…"

*Page 12, line 28. It is not clear where the term "Allan-Werle deviation plots" originated. As this reviewer understands it, the original term was Allan variance, which was extended to include Peter Werle's name after his contribution of suggesting its use in analysis of tunable diode laser spectroscopy performance. After his death, it was suggested that the term be changed to Allan-Werle variance. Suggest this term be used here.*

The term "Allan-Werle deviation plots" was changed to "plots of the square root of the Allan-Werle variance", as suggested by the referee. Therefore, the following lines were changed to the text shown below:

- line 28, page 12: "… using plots of the square root of the Allan-Werle variance (Werle et al., 1993; Onel et al., 2017a)…"
- lines 2-3, page 13: "The square root of the Allan-Werle variance, $\sigma_A(n)$, gives an estimate of the error…"
- line 9, page 13 (in the caption of Fig. 5): "…An example of the square root of the Allan-Werle variance of the absorption coefficient at 7488 $cm^{-1}$, $\sigma_A(n)$ as a function of the number of ring-down events averaged, *n* obtained in the absence of $CH_3O_2$ and in the presence of a typical acetone concentration of $8.8 \times 10^{14}$ molecule $cm^{-3}$ at 1000 mbar." Now the fig. 5 label reads "$\sigma_A(n)/cm^{-1}$" instead of "Allan-Werle deviation $\sigma_A(n)/cm^{-1}$".
- line 18, page 13 was changed to: "…Therefore, separate plots of $\sigma_A(n)$ were constructed…"
- line 2, page 14 (Table 2 title) was changed to: "…from the plots of $\sigma_A(n)$ (Fig. 5 shows an example), …"

*Page 13, line 7. Suggest adding some explanation why the acquisition rate was only 6.5 Hz. Is it not possible to have 1000 or more ring-down events per second? Perhaps give typical ring-down times. This is mentioned on page 14, line 20. Perhaps indicate how much the frequency could be increased.*

The suggested explanation was added to the text. Lines 20-21 on page 14, so the original text:
"The CRDS sensitivity could be further improved by increasing the frequency of the ring–down events and using a cavity length above the current 1.4 m length."

were replaced with:

"The relatively long ring-down times achieved here require the lasers to be blocked for several ms during which the full exponential ring-down is measured. This imposes an upper limit to the ring-down rate. The achieved rate is significantly smaller (6.5 Hz on average) for the following reasons. The width of the resonances of the optical cavity is of the order of 1 kHz, much narrower than the laser linewidth. This makes the injection of light into the cavity inefficient. Reducing the laser linewidth, e.g. with optical feedback techniques, could significantly increase the injection efficiency and the ring-down rate. Moreover, the resonance frequencies jitter and drift due to the unavoidable vibrations associated with the operation of the HIRAC chamber. The cavity length was actively modulated in order to repeatedly force coincidence of laser and resonance frequency. Due to the poor injection efficiency mentioned above, however, not every coincidence resulted in a ring-down event. Furthermore, a significant fraction of the ring-down events has to be discarded because of the passage of dust particles, moved around by the fans within the chamber, through the cavity axis.

The CRDS sensitivity could be further improved by mounting the cavity mirrors along the HIRAC length, which would result in a cavity of about 2 m length containing $CH_3O_2$ radicals, and, hence above the current 1.4 m length…"

*Page 13, line 15. Could additional optical filters be added to minimize the impact of the 254 nm photolysis radiation?*

The below sentence was added at the beginning of the paragraph above the section 3.4 (page 14):
"The use of an additional optical filter to cut-off the 254 nm light from the background of the CRDS measurements is expected to improve the CRDS sensitivity if the 254 nm lamps are used in HIRAC. The CRDS sensitivity could be further improved…"

*Page 15, lines 9 and 11. While "gradient" to describe the slope of a linear fit is technically correct, usually the term "slope" is used.*

As linear fits were used in the correlation plots the word "gradient" is adequate and was not changed to "slope".

*Page 15, line 25. Suggest "...and hence calibration of the CRDS...".*

"…and hence calibrate of the CRDS method…" was changed to "…hence calibrate the CRDS method…"

*Page 15, line 26. Suggest "...and the intercomparison is not affect by error in the rate coefficient...".*

"…and the intercomparison is not subject to any error in the rate coefficient…" was changed to "…and the intercomparison is not affected by any error in the rate coefficient…"

*Page 16, Figure 6(a). The decay of the CRDS and FAGE signals do not show the same temporal behavior. It appears there is a low pass filtering of the CRDS signals. Suggest discussing this. "Linear fit" and "orthogonal distance algorithm" are mentioned in the caption. This should be discussed in the text, with appropriate references. Also include information how the fit errors were determined. In the caption suggest "Each point is a value averaged over 3 seconds." Same suggestion for captions of Figure 7 and 8.*

Regarding the comment on Figure 6(a): "*The decay of the CRDS and FAGE signals do not show the same temporal behaviour.":*

The temporal changes in the concentration of $CH_3O_2$ measured by CRDS and FAGE are in good agreement under all the used conditions, as described in the manuscript. There are only slight discrepancies at longer decay times, which are more evident at reduced pressure (80 mbar of He + $O_2$, Figure 6(a) and 100 mbar of air, Figure 7(a)) than at 1000 mbar of air (Figure 8(a)). In Figures 6(a) and 7(a) the FAGE measurements are levelling down due to the second order kinetics going to a constant value, $[CH_3O_2] = 0$ whereas $[CH_3O_2]_{CRDS}$ continues to go down as some reaction products absorbing at the measuring wavenumber (7488 $cm^{-1}$) are changing with time. This in turn slightly changes the absorption even when the $CH_3O_2$ has reached zero concentration. The better FAGE – CRDS agreement at longer times at 1000 mbar than at 80 and 100 mbar could be due to a greater wall loss of the absorbing products at reduced pressures, where diffusion becomes more significant. However, even at 80 and 100 mbar the discrepancies noticed by the referee are minor and the FAGE – CRDS correlation plots, which incorporate all the temporal decay data show a good agreement under all conditions.

Regarding "*It appears there is a low pass filtering of the CRDS signals":*

The reviewer is right and now the following paragraph was added in line 2, page 10:
"…to extract the ring-down time, $\tau$. Filters were applied to process the ring-down events to exclude potential outliers caused by dust particles passing through the beam and false positives (when the acquisition is triggered by a transient noise spike), so that only legitimate ring-down events are taken into account."
A paragraph was added in Sect. 3.4 (see the answer to the next question of the referee 1).

Regarding *"Linear fit and orthogonal distance algorithm are mentioned in the caption. This should be discussed in the text, with appropriate references. Also include information how the fit errors were determined":*

A sentence was added in the line 9, page 15:
"…respectively. The data in the correlation plots of the $CH_3O_2$ concentrations determined by FAGE (*y*-axis) and CRDS (*x*-axis) ((Figs. 6b, 7b and 8b) were fitted using an orthogonal distance linear regression fit (Boggs et al., 1987), which accounts for errors in both the *y*- and *x*-directions. The gradient of the correlation plot at 80 mbar of He + $O_2$ (Fig. 6b)…"

Captions of figures 6, 7 and 8: "Each point is an averaged value over… " were changed to: "Each point is a value averaged over … " as suggested by the referee.

*Page 16-17, Figures 6, 7, and 8. The 80 mbar data are averaged for 3 seconds, while the 100 mbar and 1000 mbar data are averaged for 5 seconds. Suggest discussing the logic for selecting various averaging times in the text. For the intercomparison, would it not be better to average for 1 minute or more, and generate different radical concentrations by adjusting the concentrations of precursors and/or the lamp intensity, rather than use the decays to achieve different concentrations? Suggest discussing the logic of the experimental design in the body of the document.*

As explained in lines 2–4, page 15 of the MS, the comparison data were generated: (a) by delivering various concentrations of the reagents (as suggested by the referee above, so this was already done) to achieve different $[CH_3O_2]$ that decreased slowly in time due to the reagent consumption and (b) by turning off the HIRAC lamps to get a rapid decay of $[CH_3O_2]$ in time. This way the LIF method was tested in comparison with the CRDS method by monitoring both slow and rapid changes of $CH_3O_2$ concentrations and a wide range of $[CH_3O_2]$ was covered (see main manuscript). Lines 2–4, page 15 clearly explain how $[CH_3O_2]$ were generated in the comparison experiments and, hence we feel that no additional text describing this procedure is needed.

The intercomparison data were averaged over several seconds to get enough points in the rapid part of the $CH_3O_2$ kinetic decay. In order to not alter the level of noise of the data generated with the lamps on compared to the noise level of the data where the lamps were off, the same averaging time was used for all the duration of an intercomparison measurement (both periods with the lamps on and with the lamps off as shown in Figs 6a, 7a and 8a).

The paragraph below was added after line 37, page 14 to address the referee's comment regarding the difference in averaging times of the data: 3s (Fig.6) and 5 s (Figs 7 and 8).

"As the acquisition rate of CRDS (6.5 Hz in average) differed compared to the FAGE acquisition rate (in the range 1–10 Hz) the comparison data were averaged to enable comparison of [$CH_3O_2$] by the two instruments at the same moments of time. The averaging interval of time was chosen in the range 3–5 s depending on the comparison measurement to average at least 10 ring-down events over each time interval as the CRDS data were filtered to exclude outliers caused by dust particles passing through the light beam trapped in the optical cavity and the number of encountered 'dust events' varied from one experiment to another."

*Page 17, Figure 8 caption. Suggest "The measurements by FAGE are shown in red and the measurements by CRDS are plotted in black."*

The sentence clearly refers to the comparison measurement in Fig. 8(a). As in Fig. 8(a) it is shown only one measurement there is no need to change the sentence:

"The measurement by FAGE is shown in red and the measurement by CRDS is plotted in black."

*Page 17, line 33. Suggest "…FAGE detection cell (from 3.3 to 0.9 mbar when sampling from a pressure of 1000 mbar." It is not clear why three pressures are listed, or what the "respectively" refers back to. Suggest reworking this last sentence.*

Lines 33–34, page 17 were reworded:

"…in the FAGE detection cell (from 3.3 mbar, corresponding to a total HIRAC pressure of 1000, to 0.9 mbar, corresponding to a total chamber pressure of 100 or 80 mbar)."

*Page 18-19. For future reference, it is much easier for readers if the references are formatted as "hanging" paragraphs.*

We thank to the referee for the suggestion for future publications. We would like to note that the present format of the list of the references followed the journal instructions. It is expected that during any typesetting of the MS that indenting of paragraphs as suggested by the referee will be implemented.

# Author response to anonymous referee #2 on "An intercomparison of $CH_3O_2$ measurements by Fluorescence Assay by Gas Expansion and Cavity Ring–Down Spectroscopy within HIRAC (Highly Instrumented Reactor for Atmospheric Chemistry)" by L. Onel et al.

*Why did the authors measure absorption at 7488 cm-1 when Fittschen(2019) report σ (v) at 7489 cm-1? Given the results in figure 3, why do the authors consider the cross sections at the two wavelengths to be equal?*

The methane and acetone delivery led to a decrease in the ring down time due to their absorbance in the range from ~7486 to 7491 $cm^{-1}$ where the $CH_3O_2$ spectrum was measured. The measured absorption coefficient of acetone in a typical concentration of ~$9 \times 10^{14}$ molecule $cm^{-3}$ was practically constant, ~$8 \times 10^{-9}$ $cm^{-1}$ from ~7486 to 7491 $cm^{-1}$. However, $CH_4$ displays a more structured absorption spectrum in the probed region. Therefore, the $CH_3O_2$ spectrum was mapped out as a series of point measurements at fixed wavenumbers between the $CH_4$ absorption lines in the range from ~7486 to 7491 $cm^{-1}$ at 80 mbar of He + $O_2$ and 100 mbar of synthetic air (see lines 15-18, page 10). The wavenumber of 7487.98 $cm^{-1}$ was chosen for the FAGE – CRDS intercomparison measurements as there "the absorption feature is sufficiently strong and furthest in wavelength from interfering methane absorption lines…" (lines 17-18, page 10).

The following text was included in line 18, page 10:

"…was determined (Sect. 3.2). The absorption coefficient of $CH_4$ was about 7 times lower at 7487.98 cm-1 than at 7489.16 $cm^{-1}$, i.e. at the peak of the $CH_3O_2$ spectral feature where Fittschen (2019) reported $\sigma_{CH3O2}$. Therefore, 7487.98 $cm^{-1}$ (rounded to 7488 $cm^{-1}$ henceforth) was chosen as the measurement point instead of the value of 7489.16 $cm^{-1}$ used by Fittschen (2019). Each data point in Fig. 3…"

We do not consider that the value of the cross section, $\sigma_{CH3O2}$ at 7487.98 $cm^{-1}$ is equal to $\sigma_{CH3O2}$ at 7489.16 $cm^{-1}$ and the text does not state this. Lines 13 – 17, page 12 clearly explains the difference:

"To enable a comparison at 7487.98 cm-1 with the very recent measurement of Fittschen (2019), who found 2.20 × $10^{-20}$ $cm^2$ $molecule^{-1}$ at 7489.16 $cm^{-1}$, σ(7487.98 $cm^{-1}$) = 1.49 × $10^{-20}$ $cm^2$ $molecule^{-1}$ obtained in this work was multiplied by the σ(7489.16 $cm^{-1}$):σ(7487.98 $cm^{-1}$) ratio obtained by using the high resolution spectrum reported by Faragó et al. (2013) (Fig. 3). The obtained value, σ(7489.16 $cm^{-1}$) = (1.9 ± 0.3) × $10^{-20}$ $cm^2$ $molecule^{-1}$ is in reasonable agreement with the result of Fittschen (2019), σ(7489.16 $cm^{-1}$) = 2.2 × 10-20 $cm^2$ $molecule^{-1}$."

*Finally it would be helpful to have stated that the cross-section used is not the more standard integrated cross-section used by HITRAN and other databases.*

The integrated cross-section (the 'line strength') is useful when absorption lines are fitted (area under the fitted curved is proportional to line strength times concentration). For measurements at one wavelength, the 'absorption cross section' is the more appropriate, since the absorption coefficient is the concentration times the cross section. However, in case there is any confusion for those more accustomed to HITRAN, we have added in line 16, page 11:

"…, σ(7488 cm-1). Note that the cross-section used is not the more standard integrated cross-section used by HITRAN and other spectral databases. $CH_3O_2$ radicals…"

*The quantity, L, the length also requires further explanation. It should not refer to the 1.4 M value of the mirror separation in figure 2. (Morover, the comments on p14, line20-21 that one can improve the sensitivity by increasing the mirror separation, are incorrect.) The appropriate value of L is the effective path length of the sample, taking into account the diminishing concentration of CH3O2 near to and into the extensions that support the mirrors.*

As $[CH_3O_2]$ was practically homogeneous across the entire length of the mirror separation the effective cavity length was considered equal to the mirror separation, $L$ = 1.4 m.

The FAGE measurements of $CH_3O_2$ across the HIRAC diameter (1.2 m, 86% of the value of $L$) described in Sect.2.2.3 in the main manuscript showed that, indeed $[CH_3O_2]$ was practically homogeneous across the chamber diameter. Each mirror was coupled to HIRAC by a 10 cm long system of flanges (14% from L) shown in Fig. 2 in the main manuscript. Our previous publication (Onel et al. 2017a in the manuscript references), reporting CRDS measurements of $HO_2$ performed across the HIRAC width using the same coupling system of the cavity mirrors to the chamber as in the present work, investigated the potential impact of $[HO_2] = 0$ over the two 10 cm distances between the mirrors and HIRAC. In this 'worst case scenario' the analysis found that the value for the cross section of $HO_2$ agrees within 84% with the value found by considering $[HO_2]$ homogeneous along the entire $L$. We expect that the decrease in radical concentration in the proximity of the mirrors is less significant for $CH_3O_2$ than for $HO_2$ as the wall-loss for $CH_3O_2$ (upper limit of $\sim 10^{-5}$ $s^{-1}$) is significantly lower than the wall-loss for $HO_2$ (0.3-0.9 $s^{-1}$). Therefore, the expected very small decrease in $[CH_3O_2]$ over 14% of $L$ in our experiments are thought to have a negligible impact on the value of the $CH_3O_2$ cross-section yielded by the analysis.

Following the referee's comment:"*Morover, the comments on p14, line20-21 that one can improve the sensitivity by increasing the mirror separation, are incorrect*", line 21, page 14 was rephrased to clarify more its meaning:

"The CRDS sensitivity could be further improved by mounting the cavity mirrors along the HIRAC length, which would result in a cavity of about 2 m length containing $CH_3O_2$ radicals, and, hence above the current 1.4 m length…"

# Author response to anonymous referee #3 on "An intercomparison of $CH_3O_2$ measurements by Fluorescence Assay by Gas Expansion and Cavity Ring–Down Spectroscopy within HIRAC (Highly Instrumented Reactor for Atmospheric Chemistry)" by L. Onel et al.

**Minor comments**

*P2-P3: Several techniques are discussed for the measurement of peroxy radicals. The authors should also briefly discuss the use of chemical ionization mass spectrometry methods such as published in Noziere and Hanson (2017), Noziere and Vereecken (2019), Hansel et al. (2018), Jokinen et al. (2014), etc.*

We thank the referee for pointing out these additional references to include in the MS. We have now extended the introduction to discuss briefly the use of CIMS for the detection of speciated $RO_2$ radicals. The following text has been added to the MS after line 34, page 2:

"CIMS methods using reagent ions such as $H_3O^+(H_2O)n$, $NO_3^-$ and $NH_4^+$ have been employed in the simultaneous and selective detection of $RO_2$ in a number of recent studies (Noziere and Hanson, 2017; Noziere and Vereecken, 2019; Hansel et al., 2018; Jokinen et al., 2014). Volatile small $RO_2$ radicals such as $CH_3O_2$ have been selectively measured in CIMS laboratory experiments with detection limits between ~$1 \times 10^8$ –$1 \times 10^9$ molecule $cm^{-3}$ (Noziere and Hanson, 2017; Noziere and Vereecken, 2019). CIMS with $NO_3^-$ reagent ion has been employed in field measurements to record diurnal profiles of some highly oxygenated low–vapour pressure $RO_2$ radicals produced in the ozonolysis of monoterpenes peaking at a few $10^7$ molecule $cm^{-3}$ (Jokinen et al., 2014). "

*P4 L16 & P5 L19: CH4 is used during calibration experiments as a precursor for CH3O2 and is added in the Water-photolysis calibrator and the HIRAC chamber at concentrations as high as 2.5E17 molecule/cm3. Can the authors comment on the potential impact of CH4 on the quenching of CH3O in the detection cell?*

The answer to this question is given in the response to the first specific question asked by referee 1, where no quenching effect of the $CH_3O(A)$ fluorescence by $CH_4$ was found in the present experiments. Experiments were performed at several [$CH_4$] and no difference in the sensitivity factor for $CH_3O_2$ was observed. At the small mixing ratios of $CH_4$ used, and following expansion to low pressure in the FAGE fluorescence chamber, the quenching of $CH_3O(A)$ by $CH_4$ is expected to be very minor compared with that of $O_2$ or $N_2$.

*P7 Eq. 6: Please define kloss*

An explanation about kloss were added in lines 4–5, page 7:

"…the potential for a loss of $CH_3O_2$ to the walls was investigated. As circulation fans were used during all the experiments, the 'movement' of $CH_3O_2$ radicals within the chamber is in part molecular diffusion and in part convection. Therefore, the parameter $k_{loss}$ is controlled by both convection and diffusion processes. By incorporating the wall loss…"

*P6 L9-13 & P12 L4-6: What were the fitted values for kloss? Are the values inferred from the two experiments consistent with each other?*

FAGE was sampling from a point close to the chamber centre while CRDS measured $CH_3O_2$ right across the HIRAC diameter (Fig. 2 in the main text). However, the kinetic decay analysis demonstrated that wall losses were negligible in both FAGE and CRDS measurements.

The analysis of the kinetic decays monitored by the two instruments has been done in the same way for both $[CH_3O_2]_{FAGE}$ and $[CH_3O_2]_{FAGE}$ decays. The upper limit for $k_{loss}$ in the FAGE measurements was added to the text as shown in the answer to the first referee's comments:

"… the small values extracted for $k_{loss}$ (upper limit of ~ $1 \times 10^{-5}$ $s^{-1}$) fitting Eq. (6) to the FAGE data demonstrates that wall losses can be neglected…" was added on page 7, lines 11-12."

The same upper limit was obtained for $k_{loss}$ by analysing the kinetic decays measured by CRDS. The result was added in line 6, page 12:

"…are statistical uncertainties. The values extracted for $k_{loss}$ by fitting Eq. (9) to the CRDS data were small and similar to the values obtained by fitting Eq. (6) to the kinetic decays monitored by FAGE. An upper limit of ~ $1 \times 10^{-5}$ $s^{-1}$ was obtained for $k_{loss}$ in both FAGE and CRDS measurements, showing that wall losses are negligible. From fitting…"

*P6 L22: "1E-10" should read "1E-9"*

"1E-10" was corrected to "1E-9"

*P15 L9-12 & L17-18 & L21-22: The authors show that correlation plots between FAGE and CRDS exhibit slopes that are close to unity. However, the y-intercepts of the regression lines are not discussed. Were the intercepts not statistically significant?*

The *y*-intercepts of the FAGE – CRDS correlation plots (Figs. 6b, 7b and 8b) have either a small negative value (Fig. 6b) or a positive value (Fig. 7b and 8b). We believe that the main source for the *y*-intercept values derived by the linear fit to the data is the method used to determine the background of the CRDS measurements. The background ring-down time (the ring-down time in the $CH_3O_2$ absence, $\tau_0$) increased slightly during the time intervals with the lamps on due to the slow depletion of the reagents (methane or acetone). However, $\tau_0$ could not be measured simultaneously with the ring-down time in the presence of the $CH_3O_2$ radicals, $\tau$. Therefore, the background was regularly monitored by turning the lamps off, as explained in lines 9 – 10, page 10:

"As it is not possible to measure $\tau_0$ and $\tau$ simultaneously, the background was monitored regularly during each experiment by switching off the photolysis lamps and allowing the signal to return to the baseline."

We also added a new paragraph describing the impact of the acetone and methane absorption on $\tau_0$ to the main text (see the answer to the first specific comment of the referee 1).

The background in the FAGE measurements could not also be recorded simultaneously with the $CH_3O_2$ FAGE signal as it required the FAGE instrument measured off-line. Therefore, the off-line measurement was taken at the end of each on-line measurement. However, the FAGE measurement background was independent on any changes in the composition of the HIRAC gas mixture. Therefore, we believe that the source of the linear regression intercepts mentioned by the referee comes from the uncertainties associated with the determination of the CRDS measurement background as explained above. The intercepts are not significant as their values are only a few percent from the largest $[CH_3O_2]$ shown in each correlation plot.

*P16 Figures 6-7: When the lamps are turned off, (1) the CRDS measurements seem to decrease to lower values than FAGE and (2) the FAGE measurements seem to reach a plateau more rapidly than the CRDS. Could the authors comment on this?*

As it was not possible to measure $\tau_0$ and $\tau$ simultaneously the background ring-down time was recorded regularly by turning off the chamber lamps to account for the slow decrease in the reagent (methane or acetone) concentrations (*vide supra*). The method led to typical small deviations of the baseline of the CRDS kinetic decays from zero and to the slight differences between the baselines of the $[CH_3O_2]_{FAGE}$ decay and $[CH_3O_2]_{CRDS}$ decay mentioned by the referee.

The two referee's observations are coupled to each other – the $[CH_3O_2]_{CRDS}$ continuing to go down, and $[CH_3O_2]_{FAGE}$ levelling off quicker. The FAGE measurement levelling is due to the second order kinetics going to a constant value, $[CH_3O_2] = 0$ whereas $[CH_3O_2]_{CRDS}$ continues to go down as some reaction products absorbing at the measuring wavenumber (7488 $cm^{-1}$) are changing with time. This in turn slightly changes the absorption even when the $CH_3O_2$ has reached zero concentration. Both these effects are more evident at 80 and 100 mbar than at 1000 mbar. The better FAGE – CRDS agreement at longer times at 1000 mbar than at 80 and 100 mbar could be due to a greater wall loss of the absorbing products at reduced pressures, where diffusion becomes more significant. However, even at 80 and 100 mbar the discrepancies noticed by the referee are minor and the FAGE – CRDS correlation plots, which incorporate all the temporal decay data show a good agreement under all conditions.

# An intercomparison of $CH_3O_2$ measurements by Fluorescence Assay by Gas Expansion and Cavity Ring–Down Spectroscopy within HIRAC (Highly Instrumented Reactor for Atmospheric Chemistry)

Lavinia Onel[1], Alexander Brennan[1], Michele Gianella[2], James Hooper[1], Nicole Ng[2], Gus Hancock[2], Lisa Whalley[1,3], Paul W. Seakins[1,3], Grant A. D. Ritchie[2], Dwayne E. Heard[1,3]

[1] School of Chemistry, University of Leeds, Leeds, LS2 9JT, UK
[2] Department of Chemistry, Physical and Theoretical Chemistry Laboratory, University of Oxford, Oxford, OX1 3QZ, UK
[3] National Centre for Atmospheric Science, University of Leeds, Leeds, LS2 9JT, UK

*Correspondence to*: Lavinia Onel (chmlo@leeds.ac.uk); Paul Seakins (p.w.seakins@leeds.ac.uk); Grant Ritchie (grant.ritchie@chem.ox.ac.uk); Dwayne Heard (d.e.heard@leeds.ac.uk)

**Abstract**

Simultaneous measurements of $CH_3O_2$ radical concentrations have been performed using two different methods in the Leeds HIRAC (Highly Instrumented Reactor for Atmospheric Chemistry) chamber at 295 K and in 80 mbar of a mixture of 3:1 He:$O_2$ and 100 mbar or 1000 mbar of synthetic air. The first detection method consisted of the indirect detection of $CH_3O_2$ using the conversion of $CH_3O_2$ into $CH_3O$ by excess NO with subsequent detection of $CH_3O$ by fluorescence assay by gas expansion (FAGE). The FAGE instrument was calibrated for $CH_3O_2$ in two ways. In the first method, a known concentration of $CH_3O_2$ was generated using the 185 nm photolysis of water vapour in synthetic air at atmospheric pressure followed by the conversion of the generated OH radicals to $CH_3O_2$ by reaction with $CH_4/O_2$. This calibration can be used for experiments performed in HIRAC at 1000 mbar in air. In the second method, calibration was achieved by generating a near steady-state of $CH_3O_2$ and then switching off the photolysis lamps within HIRAC and monitoring the subsequent decay of $CH_3O_2$ which was controlled via its self-reaction, and analysing the decay using second order kinetics. This calibration could be used for experiments performed at all pressures. In the second detection method, $CH_3O_2$ has been measured directly using Cavity Ring-Down Spectroscopy (CRDS) using the absorption at 7487.98 $cm^{-1}$ in the $A \leftarrow X$ ($\nu_{12}$) band with the optical path along the ~1.4 m chamber diameter. Analysis of the second-order kinetic decays of $CH_3O_2$ by self-reaction monitored by CRDS has been used for the determination of the $CH_3O_2$ absorption cross section at 7487.98 $cm^{-1}$, both at 100 mbar of air and at 80 mbar of a 3:1 He:$O_2$ mixture, from which $\sigma_{CH3O2}$ = (1.49 ± 0.19) × $10^{-20}$ $cm^2$ $molecule^{-1}$ was determined for both pressures. The absorption spectrum of $CH_3O_2$ between 7486 and 7491 $cm^{-1}$ did not change shape when the total pressure was increased to 1000 mbar, from which we determined that $\sigma_{CH3O2}$ is independent of pressure over the pressure range 100–1000 mbar in air. $CH_3O_2$ was generated in HIRAC using either the photolysis of $Cl_2$ with UV black lamps in the presence of $CH_4$ and $O_2$ or the photolysis of acetone at 254 nm in the presence of $O_2$. At 1000 mbar of synthetic air the correlation plot of $[CH_3O_2]_{FAGE}$ against $[CH_3O_2]_{CRDS}$ gave a gradient of 1.09 ± 0.06. At 100 mbar of synthetic air ~~the gradient of~~ the FAGE – CRDS correlation plot had a gradient of 0.95 ± 0.02 and at 80 mbar of 3:1 He:$O_2$ mixture the correlation plot gradient was 1.03 ± 0.05. These results provide a validation of the FAGE method to determine concentrations of $CH_3O_2$.

## 1 Introduction

Methyl peroxy ($CH_3O_2$) radicals are important intermediates during atmospheric oxidation (Orlando and Tyndall, 2012) and combustion chemistry (Zador et al., 2011), and are produced mainly by the oxidation of $CH_4$ and larger hydrocarbons followed by the termolecular reaction between the $CH_3$ radical, $O_2$ and a third body (Reaction R1).

$$CH_3 + O_2 + M \rightarrow CH_3O_2 + M \qquad (R1)$$

In environments influenced by anthropogenic $NO_x$ emissions, $CH_3O_2$ predominantly reacts with NO to produce $NO_2$ and $CH_3O$ (Reaction R2).

$$CH_3O_2 + NO \rightarrow CH_3O + NO_2 \quad (R2)$$

$CH_3O$ subsequently reacts with $O_2$ (Reaction R3) to generate $HO_2$, which in turn oxidises another NO molecule to $NO_2$ (Reaction R4). The subsequent photolysis of $NO_2$ leads to the formation of tropospheric ozone, an important constituent of photochemical smog.

$$CH_3O + O_2 \rightarrow CH_2O + HO_2 \quad (R3)$$

$$HO_2 + NO \rightarrow OH + NO_2 \quad (R4)$$

In remote, clean environments, i.e. under low $NO_x$ levels, $CH_3O_2$ is significantly removed by its self-reaction (Reaction R5) and the cross-reactions with $HO_2$ and other organic peroxy radicals ($RO_2$) (Tyndall et al., 2001).

$$CH_3O_2 + CH_3O_2 \rightarrow CH_3OH + CH_2O + O_2 \quad (R5a)$$

$$CH_3O_2 + CH_3O_2 \rightarrow CH_3O + CH_3O + O_2 \quad (R5b)$$

Recently the reaction of $CH_3O_2$ with OH was measured to be fast (Fittschen, 2019;Yan, 2016) and provides an additional loss route for $CH_3O_2$ under low $NO_x$ conditions (Fittschen et al., 2014;Assaf et al., 2017). As $CH_3O_2$ is formed by the oxidation of $CH_4$, one of the most abundant tropospheric trace gases, as well as by the oxidation of other volatile organic compounds, it is predicted by numerical models to be the most abundant $RO_2$ species in the atmosphere. Although $CH_3O_2$ has not (yet) been selectively measured in the atmosphere, its concentration has been estimated using atmospheric models to peak at ~$10^7$ – $10^8$ molecule $cm^{-3}$ during the daytime (Whalley et al., 2010;Whalley et al., 2011;Whalley et al., 2018).

At present, $CH_3O_2$ is not measured selectively in the atmosphere by any direct or indirect method. The sum of $HO_2$ and all $RO_2$ species, $[HO_2] + \sum_i [RO_{2,i}]$, and separately, the sum of $RO_2$, $\sum_i [RO_{2,i}]$, have been measured in the atmosphere using a range of indirect methods. Onel et al. (2017a) presents an overview of these methods, such as the peroxy radical chemical amplifier (PERCA) (Cantrell et al., 1984;Hernandez et al., 2001;Green et al., 2006;Miyazaki et al., 2010;Wood et al., 2017), $RO_x$ chemical conversion – CIMS (chemical ionisation mass spectrometry) ($RO_x$MAS) (Hanke et al., 2002) and $RO_x$ chemical conversion – LIF (laser induced fluorescence) ($RO_x$LIF) (Fuchs et al., 2008;Whalley et al., 2013). $RO_x$LIF uses LIF detection of OH at low pressure, known as fluorescence assay by gas expansion (FAGE) and has been employed for partially speciated $RO_2$ detection, distinguishing between the sum of alkene, aromatic and long-chain alkane-derived $RO_2$ radicals and the sum of short-chain alkane-derived $RO_2$ radicals (Whalley et al., 2013;Whalley et al., 2018).

CIMS methods using reagent ions such as $H_3O^+(H_2O)n$, $NO_3^-$ and $NH_4^+$ have been employed in the simultaneous and selective detection of $RO_2$ in a number of recent studies (Noziere and Hanson, 2017;Noziere and Vereecken, 2019;Hansel et al., 2018;Jokinen et al., 2014). Volatile small $RO_2$ radicals such as $CH_3O_2$ have been selectively measured in CIMS laboratory experiments with detection limits between ~$1 \times 10^8$ –$1 \times 10^9$ molecule $cm^{-3}$ (Noziere and Hanson, 2017). CIMS with $NO_3^-$ reagent ion has been employed in field measurements to record diurnal profiles of some highly oxygenated low–vapour pressure $RO_2$ radicals produced in the ozonolysis of monoterpenes peaking at a few $10^7$ molecule $cm^{-3}$ (Jokinen et al., 2014).

Many of the early laboratory studies of the $CH_3O_2$ radical reactions employed UV-absorption spectroscopy to monitor the $B \leftarrow X$ band centred around 240 nm, that is common to alkyl $RO_2$ species (Wallington et al., 1992;Tyndall et al., 2001). The similarity of the broad featureless UV-absorption spectra of $RO_2$ radicals made it challenging to distinguish between the individual $RO_2$ species, particularly in a mixture (Orlando and Tyndall, 2012). The sensitivity of UV-absorption spectroscopy

is quite low, for example a minimum detectable absorption of $5 \times 10^{-3}$, corresponding to $4 \times 10^{12}$ molecule cm$^{-3}$ $CH_3O_2$ was reported (Sander and Watson, 1980). The $A \leftarrow X$ electronic transition of $RO_2$ in the near IR (NIR) displays more structured spectra than the UV region, allowing a selective identification of $RO_2$ radicals. However the $A \leftarrow X$ transition is weaker than the $B \leftarrow X$ transition and multipass arrangements have been used to improve the detection sensitivity. A step-scan Fourier Transform Infrared spectrometer (Huang et al., 2007) operated using a multipass White cell has been used to detect a number of $RO_2$ species, including $CH_3O_2$, with a typical minimum detectable absorbance of $\sim 1 \times 10^{-4}$, corresponding to a limit of detection (*LOD*) of $\sim 1 \times 10^{13}$ molecule cm$^{-3}$ for most $RO_2$ species studied. The use of cavity ring-down spectroscopy (CRDS) further improves the sensitivity of the $RO_2$ detection due to the significantly longer pathlengths that can be realized and to the coupling of high performance NIR lasers, detectors and optical components. For example, an absorbance detection limit of less than $1 \times 10^{-6}$ has been obtained by using cavity mirrors of a maximum reflectivity of 99.995% (Atkinson and Spillman, 2002).

The CRDS technique has been used under both ambient and jet-cooled conditions to provide insight into the molecular structure of $CH_3O_2$ and more complex $RO_2$, and to selectively measure [$RO_2$] in the laboratory (Sharp et al., 2008;Kline and Miller, 2014;Pushkarsky et al., 2000;Farago et al., 2013;Atkinson and Spillman, 2002;Sprague et al., 2013). Good agreement has been found between the experimental spectrum of $CH_3O_2$ in the range between ~7200–8600 cm$^{-1}$ (~1.18–1.40 μm) measured using pulsed CRDS at typically 200 mbar of $N_2$:$O_2$ = 1.5:1.0 and theoretical predictions (Chung et al., 2007;Sharp et al., 2008). The origin band of the $A \leftarrow X$ transition has been located at 7382.8 cm$^{-1}$ and a value of $2.7 \times 10^{-20}$ cm$^2$ molecule$^{-1}$ has been estimated for the absorption cross section at this wavenumber (Pushkarsky et al., 2000;Chung et al., 2007). A weaker absorption band has been found at 7488 cm$^{-1}$ and assigned to a transition involving the methyl torsion ($\nu_{12}$) (Pushkarsky et al., 2000;Chung et al., 2007). By using the $CH_3O_2$ spectrum measured by Pushkarsky et al. (2000) from 7300–7700 cm$^{-1}$, which covers both the origin band and the band involving the methyl torsional mode, a value of ca. $1.0 \times 10^{-20}$ cm$^2$ molecule$^{-1}$ is estimated for the maximum cross section for the $\nu_{12}$ transition, $\sigma_{max}(\nu_{12})$. A few years later, (Atkinson and Spillman, 2002) measured $\sigma_{max}(\nu_{12}) = (1.5 \pm 0.8) \times 10^{-20}$ cm$^2$ molecule$^{-1}$ at 27 mbar $N_2$:$O_2$ = 4:1 using continuous-wave (cw) CRDS. Very recent cw-CRDS studies reported $\sigma_{max}(\nu_{12}) = 2.2 \times 10^{-20}$ cm$^2$ molecule$^{-1}$ at 67 mbar of a He + $O_2$ mixture (Fittschen, 2019) and no dependence of $\sigma_{max}(\nu_{12})$ on pressure over the range from 67 to 133 mbar (Farago et al., 2013).

Recently we have developed a new method for the selective and sensitive detection of $CH_3O_2$ using the conversion of $CH_3O_2$ to $CH_3O$ with excess NO followed by $CH_3O$ detection by FAGE with laser excitation at *ca*. 298 nm (Onel et al., 2017b). The *LOD* for the method whilst sampling from atmospheric pressure is $\sim 4.0 \times 10^8$ molecule cm$^{-3}$ for a signal-to-noise ratio of 2 and 5 min averaging time; the *LOD* is reduced to $\sim 1.0 \times 10^8$ molecule cm$^{-3}$ by averaging over 1 hour. Therefore, the method has potential to be used in the measurement of atmospheric levels of $CH_3O_2$ in clean environments where [$CH_3O_2$] has been calculated to be a few $10^8$ molecule cm$^{-3}$ (Whalley et al., 2010;Whalley et al., 2011). As LIF is not an absolute method of detection, FAGE instruments require calibration. Two methods of calibration for $CH_3O_2$ have been used (Onel et al., 2017b): the 184.9 nm photolysis of water vapour in the presence of excess $CH_4$ and the kinetics of the second-order decay of $CH_3O_2$ via its self–reaction observed in the Highly Instrumented Reactor for Atmospheric Chemistry (HIRAC). Good agreement was found, *i.e*. the calibration factors obtained using the two methods had overlapping error limits at the $1\sigma$ level.

However, radicals are difficult to detect accurately and, particularly as FAGE is not an absolute and direct method, may be subject to systematic errors and, hence require validation using complementary methods. Recently we intercompared measurements of $HO_2$ concentrations by the indirect FAGE method and the direct and absolute CRDS method within HIRAC, and demonstrated good agreement, within 10% and 16% at 150 mbar and 1000 mbar, respectively (Onel et al., 2017b), which validates the FAGE method for $HO_2$. In this work, $CH_3O_2$ measurements by FAGE and CRDS within HIRAC are intercompared at 80 mbar for a mixture of 3:1 He:$O_2$ and at 100 mbar and 1000 mbar for air.

## 2 Experimental

### 2.1 $CH_3O_2$ generation in HIRAC

The HIRAC chamber (Glowacki et al., 2007) is constructed from 304 stainless steel and has an internal volume of ~2.25 $m^3$, the contents of which are homogenised by four mixing fans. Eight 50 mm diameter quartz tubes are mounted radially inside the chamber and extend along its ~2 m length. Each of the eight tubes house a UV lamp that is used to initiate chemical reactions. The lamps can be changed to different wavelength outputs depending on the chemical precursors to be used. The FAGE instrument is connected to the HIRAC chamber through an ISO-K160 flange with an O-ring compression fitting to allow the inlet distance from the wall of the chamber to be varied. The 380 mm long inlet allows the instrument to sample well away from the inner walls of the HIRAC chamber and avoid chemical processes at the metal surface. Because the FAGE system removes gas from the HIRAC chamber, a constant flow of synthetic air is introduced into the chamber to maintain a constant pressure. The CRDS setup is described in Sect. 2.3.

The experiments were conducted inside the HIRAC chamber at 295 K using three different pressure / gas mixtures. The first used 80 mbar total pressure of helium (BOC, >99.99 %) and oxygen (BOC, >99.999 %) in the ratio of $He:O_2$ = 3:1. The second and third mixtures both used synthetic air obtained by mixing oxygen with nitrogen (BOC, > 99.998 %) in the ratio $N_2:O_2$ = 4:1 at 100 and 1000 mbar total pressure, respectively. $CH_3O_2$ was generated in the chamber by photolysing one of two precursor gas mixtures. The first $CH_3O_2$ precursor system was a mixture of $Cl_2$ (Sigma Aldrich, ≥ 99.5 %) and $CH_4$ (BOC, CP grade, 99.5 %), where the $Cl_2$ was photolysed at ~365 nm (Phillips, TL-D36W/BLB, λ = 350–400 nm) to generate $CH_3O_2$ *via* the reactions:

$$Cl_2 + h\nu\ (365\ nm) \rightarrow Cl + Cl \quad (R6)$$

$$CH_4 + Cl \rightarrow CH_3 + HCl \quad (R7)$$

$$CH_3 + O_2 + M \rightarrow CH_3O_2 + M \quad (R1)$$

Typical reagent concentrations were $[CH_4]$ = 1.2–2.5 × $10^{16}$ molecule $cm^{-3}$ and $[Cl_2]$ = 1.1–5.5 × $10^{15}$ molecule $cm^{-3}$. The second method used the photolysis of acetone (Sigma Aldrich, HPLC grade, ≥ 99.9 %) at 254 nm (GE G55T8/OH 7G lamps) to produce $CH_3O_2$ *via* (R9) and (R10) followed by (R1):

$$(CH_3)_2CO + h\nu\ (254\ nm) \rightarrow 2CH_3 + CO \quad (R8)$$

$$(CH_3)_2CO + h\nu\ (254\ nm) \rightarrow CH_3 + CH_3CO \quad (R9)$$

Typical initial concentrations were $[(CH_3)_2CO]$ = 8.8 × $10^{14}$ molecule $cm^{-3}$. In the FAGE calibration experiments using the kinetic decays $[Cl_2]_0$ = 1.1 × $10^{14}$ molecule $cm^{-3}$ with $CH_4$ at one of two concentrations: 2.5 × $10^{16}$ molecule $cm^{-3}$ and 2.5 × $10^{17}$ molecule $cm^{-3}$. In the kinetic experiments performed to determine the absorption cross section of $CH_3O_2$ at 7487.98 $cm^{-1}$, $[Cl_2]_0$ = 1.1 × $10^{14}$ molecule $cm^{-3}$ and $[CH_4]_0$ = 2.5 × $10^{16}$ molecule $cm^{-3}$ at 80 mbar $He:O_2$ = 3:1 and $[Cl_2]_0$ = 1.0 × $10^{15}$ molecule $cm^{-3}$ and $[CH_4]_0$ = 2.4 × $10^{16}$ molecule $cm^{-3}$ at 100 mbar $N_2:O_2$ = 4:1.

### 2.2 FAGE instrument and calibration for $CH_3O_2$

The FAGE instrument in HIRAC has been described in detail previously (Winiberg et al., 2015;Onel et al., 2017a;Onel et al., 2017b). The instrument has a ~ 1 m long black anodised aluminium sampling tube with an inner diameter of 50 mm. The interior of the tube is held at a low pressure (3.3 mbar for a HIRAC pressure, $p_{HIRAC}$ of 1000 mbar of synthetic air and 0.9 mbar for $p_{HIRAC}$ = 100 mbar synthetic air and $p_{HIRAC}$ = 80 mbar mixture of $He:O_2$ = 3:1) ~~of 3.3 mbar~~ and draws sample gas in through

a 1 mm diameter pinhole mounted on one end of the tube at a rate of ~35 SLM. Two fluorescence cells are integrated into the tube, the centre of the first cell is ~300 mm from the pinhole, and the centre of the second cell is a further ~300 mm downstream, followed by a line of tubing that is connected to a rotary backed roots blower pump system (Leybold Trivac D40B and Ruvac WAU 251). The first cell is used to detect OH radicals but is not relevant to this work and is not discussed further, whereas the second cell is used for the $CH_3O_2$ measurements detailed here. The $CH_3O_2$ radicals sampled through the FAGE pinhole at 1000 mbar in HIRAC reached the detection region in about 85 ms. High purity NO (BOC, N2.5 nitric oxide) is injected at 2.5 sccm using a mass flow controller (Brooks 5850S) into the centre of the gas flow ~25 mm prior to the second cell to convert $CH_3O_2$ radicals into $CH_3O$. Pulsed laser light at 297.79 nm is directed through the cell and propagates perpendicular to the gas flow and is used to excite the $A^2A_1(v_3' = 3) \leftarrow X^2E(v_3'' = 0)$ transition of $CH_3O$. The off resonant, red shifted fluorescence (320-430 nm) from $CH_3O$ ($A$) is subsequently detected by a microchannel plate photomultiplier (Photek PMT325) using photon counting. Measurements are made at an excitation wavelength of 297.79 + 2.5 nm in order to determine the laser background, which is subtracted to leave only signal due to $CH_3O$ fluorescence.

The FAGE technique is not absolute and therefore determination of the calibration factor, $C_{CH_3O_2}$ (counts cm$^3$ molecule$^{-1}$ s$^{-1}$ mW$^{-1}$), is required, to convert the measured signal, $S_{CH_3O_2}$, (counts s$^{-1}$ mW$^{-1}$), to the $CH_3O_2$ concentration:

$$[CH_3O_2] = \frac{S_{CH_3O_2}}{C_{CH_3O_2}} \quad (1)$$

### 2.2.1 Calibration at atmospheric pressure - $H_2O$ vapour photolysis in the presence of excess $CH_4$

This calibration procedure has been described in detail previously (Winiberg et al., 2015;Onel et al., 2017b), as such only important points are represented here. $CH_3O_2$ radicals were generated by photolysing water vapour in air (BOC, synthetic BTCA 178) at 184.9 nm to produce OH radicals, which then reacted with methane (BOC, CP grade, 99.5 %) to produce $CH_3O_2$:

$$H_2O + h\nu\ (185\ nm) \rightarrow OH + H \quad (R10)$$

$$OH + CH_4 \rightarrow CH_3 + H_2O \quad (R11)$$

$$CH_3 + O_2 + M \rightarrow CH_3O_2 + M \quad (R1)$$

The subsequent air/radical mixture was then sampled by the FAGE instrument. The concentration of $CH_3O_2$ generated is given by:

$$[CH_3O_2] = [OH] = [H_2O] \cdot \sigma \cdot \Phi \cdot F \cdot t \quad (2)$$

where σ is the absorption cross section of water vapour at 184.9 nm, (7.22 ± 0.22) × 10$^{-20}$ cm$^2$ molecule$^{-1}$ (Cantrell et al., 1997;Creasey et al., 2000), Φ is the photo-dissociation quantum yield of OH at 184.9 nm (unity), $t$ is the residence time of the gas in the photolysis field, which is ~16.6 and ~8.3 ms at 20 and 40 SLM respectively, and $F$ is the lamp flux at 184.9 nm. The product $F \cdot t$ is determined using chemical actinometry (Winiberg et al., 2015). The 184.9 nm photon flux, $F$, is proportional to the electrical current supplied to the photolysis lamp and is varied to produce a range of $CH_3O_2$ radical concentrations. A typical calibration plot of the FAGE LIF signal vs. generated $[CH_3O_2]$ calculated using Eq. (2) is shown in the Supplementary Information (SI), Figure S21. An average of four calibrations gave $C_{CH_3O_2}$ = (8.03 ± 1.37) × 10$^{-10}$ counts cm$^3$ molecule$^{-1}$ s$^{-1}$ mW$^{-1}$ where the error represents the overall uncertainty (17%) calculated using the statistical error (7%) and the systematic error (16%) at 1$\sigma$ level (Onel et al., 2017b).

### 2.2.2 Calibration using kinetics of the $CH_3O_2$ temporal decay

The calibration described in the previous section is only valid when FAGE is sampling at atmospheric pressure. However, when sampling from lower pressures, as described in Sect. 2.1, the FAGE cell pressure decreases (0.9 mbar sampling from 100 mbar) and the calibration is no longer valid. An alternative calibration procedure using the kinetics of the $CH_3O_2$ self-reaction inside the HIRAC chamber allowed the FAGE instrument to be calibrated under the same conditions of pressure as the intercomparison experiments, including at lower pressures. Table 1 shows the sensitivity factors, $C_{CH_3O_2}$, obtained for each set of chamber conditions. Radicals were generated in the chamber in the same manner as those described in Sect. 2.1. However, instead of measuring steady state radical concentrations, the lamps were switched off and on at ~120 s intervals to produce a series of second–order decays, typically 4 per experiment, in which $CH_3O_2$ undergoes loss via self-reaction:

$$CH_3O_2 + CH_3O_2 \rightarrow CH_3OH + CH_2O + O_2 \quad \text{(R5a)}$$

$$CH_3O_2 + CH_3O_2 \rightarrow CH_3O + CH_3O + O_2 \quad \text{(R5b)}$$

Assuming no wall loss for $CH_3O_2$, the kinetic decays can be described by the integrated second order rate equation:

$$\frac{1}{[CH_3O_2]_t} = \frac{1}{[CH_3O_2]_0} + 2 \cdot k_{obs} \cdot \Delta t \quad (3)$$

where $[CH_3O_2]_t$ is the radical concentration at time $t$ of the decay, $[CH_3O_2]_0$ is the initial concentration at the time~~,~~ $t_0$, when the lamps are switched off, $\Delta t = t - t_0$ and $k_{obs}$ is the observed rate coefficient. The observed rate coefficient is larger than the second order rate coefficient of just the $CH_3O_2$ recombination reaction (R5) as the methoxy radicals generated by channel R5.b react rapidly with oxygen present in large excess to produce $HO_2$ (R3), which in turn reacts with $CH_3O_2$ (R12).

$$CH_3O + O_2 \rightarrow CH_2O + HO_2 \quad \text{(R3)}$$

$$CH_3O_2 + HO_2 \rightarrow 0.9CH_3OOH + 0.1CH_2O + 0.1H_2O + O_2 \quad \text{(R12)}$$

As each $HO_2$ radical consumes rapidly one $CH_3O_2$ species on the time scale of the reaction R5, the $CH_3O_2$ decay is described by second order kinetics ~~This further reaction of $CH_3O_2$ with $HO_2$ however does not stop the decay analysis, as in previous publications~~ (Sander and Watson, 1980); (Sander and Watson, 1981;McAdam et al., 1987;Kurylo and Wallington, 1987;Jenkin et al., 1988;Simon et al., 1990), with $k_{obs} = k_5(1 + r_{5b})$, where $r_{5b}$ is the branching ratio for the channel R5b. By using the IUPAC recommendations (Atkinson et al., 2006): $k_5 = (3.5 \pm 1.0) \times 10^{-13}$ molecule$^{-1}$ cm$^3$ s$^{-1}$ and $r_{5b} = 0.37 \pm 0.06$, a value of $4.8 \times 10^{-13}$ molecule$^{-1}$ cm$^3$ s$^{-1}$ is obtained for $k_{obs}$.

Modelling of the decay process with a variety of $CH_3O_2$ and $HO_2$ concentrations after the lamps were switched off and following the establishment of steady state conditions showed that Eq. (3) was valid within experimental error. With ~~the rate constant for the bimolecular process R5 taken from the IUPAC as~~ $k_5 = 3.5 \times 10^{-13}$ molecule$^{-1}$ cm$^3$ s$^{-1}$ (Atkinson et al., 2006), a faster observed rate constant (defined by Eq. (3)) was obtained from the model with a value, $4.9 \times 10^{-13}$ molecule$^{-1}$ cm$^3$ s$^{-1}$ consistent with that recommended by IUPAC, $(4.8 \pm 0.6) \times 10^{-13}$ molecule$^{-1}$ cm$^3$ s$^{-1}$ ($1\sigma$ uncertainty; Atkinson et al., 2006). Substituting Eq. (1) into Eq. (3) allows the measured signal over the decay to be related to the instrument sensitivity by:

$$\frac{1}{(S_{CH_3O_2})_t} = \frac{1}{(S_{CH_3O_2})_0} + \frac{2 \cdot k_{obs} \cdot \Delta t(t - t_0)}{C_{CH_3O_2}} \quad (4)$$

where $(S_{CH_3O_2})_t$ and $(S_{CH_3O_2})_0$ are the FAGE signal at time $t$ and $t_0$ respectively. Taking the reciprocal of Eq. (4) gives:

$$(S_{CH_3O_2})_t = \left( \frac{1}{(S_{CH_3O_2})_0} + \frac{2 \cdot k_{obs} \cdot \Delta t(t - t_0)}{C_{CH_3O_2}} \right)^{-1} \quad (5)$$

which is then used to fit to the experimental data with $k_{obs}$ fixed to the value recommended by IUPAC for 298 K, $4.8 \times 10^{-13}$ molecule$^{-1}$ cm$^3$ s$^{-1}$, using the Levenberg-Marquardt algorithm. Figure 1 shows an example $CH_3O_2$ self-reaction decay trace obtained at 1000 mbar, where the red line shows the result of the fitting process.

However, as the HIRAC chamber is constructed from steel, the potential for a loss of $CH_3O_2$ to the walls was investigated. As circulation fans were used during all the experiments, the 'movement' of $CH_3O_2$ radicals within the chamber is in part molecular diffusion and in part convection. Therefore, the parameter $k_{loss}$ is controlled by both convection and diffusion processes. By incorporating the wall loss as a first-order process Eq. (5) becomes:

$$(S_{CH_3O_2})_t = \left( \left( \frac{1}{(S_{CH_3O_2})_0} + \frac{2 \cdot k_{obs}}{k_{loss} \cdot C_{CH_3O_2}} \right) \times \exp(k_{loss} \cdot \Delta t(t - t_0)) - \left( \frac{2 \cdot k_{obs}}{k_{loss} \cdot C_{CH_3O_2}} \right) \right)^{-1} \quad (6)$$

Fitting Eqs. (5) and (6) to the experimental data is also shown in Fig. 1. The extracted values for the sensitivity factor are the same for the fit without and with wall loss included: $C_{CH3O2} = (1.17 \pm 0.04) \times 10^{-9}$ counts cm$^3$ molecule$^{-1}$ s$^{-1}$ mW$^{-1}$ (statistical errors at $1\sigma$ level). The close overlap of the fits without and with wall loss included and the small values extracted for $k_{loss}$ (upper limit of ~ $1 \times 10^{-5}$ s$^{-1}$) ~~the negligible values extracted for $k_{loss}$~~ fitting Eq. (6) demonstrates that wall losses are very small and can be neglected. This is evidenced further by the lack of an observable radical gradient across the chamber diameter as shown in Fig. S5~~4~~ in the Supplementary Information. In addition, modelling the $CH_3O_2$ decays including a wall loss for $HO_2$ in the range of measured values 0.03–0.09 s$^{-1}$ (Onel et al. 2017a), showed a minor impact of the wall loss of $HO_2$ on $k_{obs}$, i.e. $k_{obs}$ within 98–95 % agreement with the IUPAC preferred value, $(4.8 \pm 0.6) \times 10^{-13}$ molecule$^{-1}$ cm$^3$ s$^{-1}$ ($1\sigma$ uncertainty; Atkinson et al., 2006).

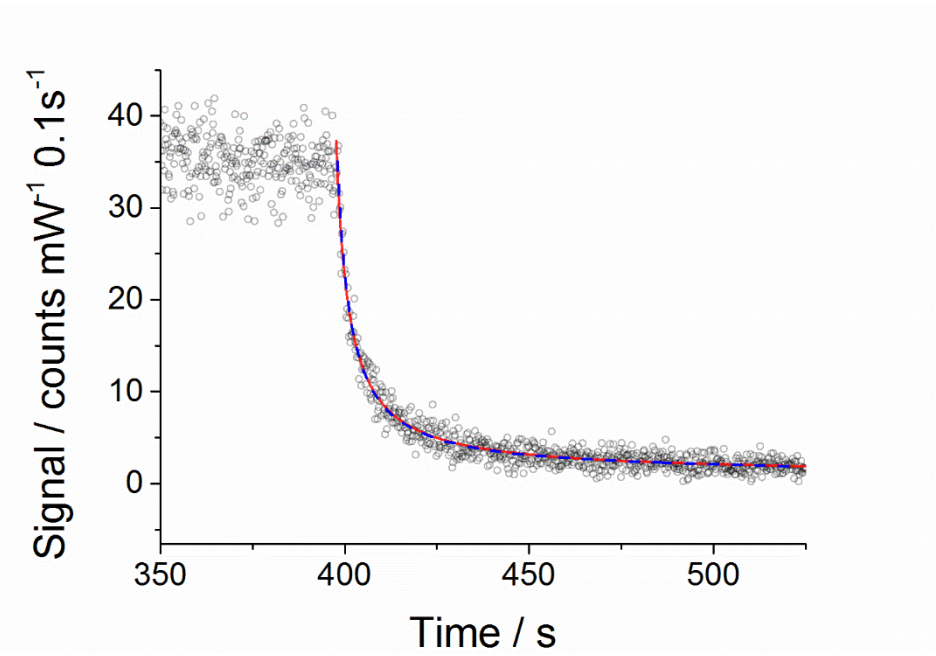

**Figure 1.** An example of a second -order decay of the FAGE $CH_3O_2$ signal (normalized for laser power fluctuations) with 0.1 second time resolution (black open circles) recorded at 295 K and a 1000 mbar air mixture. $CH_3O_2$ was generated using $[Cl_2]$ ~$1.1 \times 10^{14}$ molecule $cm^{-1}$ and $[CH_4]$ ~$2.5 \times 10^{16}$ molecule $cm^{-3}$. At time zero (~400 s) the photolysis lamps were turned off to allow the radicals to decay. The data were fitted to Eq. (5) (excluding the wall loss rate, $k_{loss}$; red line) and Eq. (6) (including $k_{loss}$; blue dashed line) using the Levenberg-Marquardt algorithm. The obtained value for the sensitivity factor was the same for both fits: $C_{CH3O2}$ = (1.17 ± 0.04) × $10^{-9}$ counts $cm^3$ $molecule^{-1}$ $s^{-1}$ $mW^{-1}$. ~~Fitting of Eq. (5) to the data (red line) gave $C_{CH3O2}$ = (1.18 ± 0.02) × $10^{-10}$ counts $cm^3$ $molecule^{-1}$ $s^{-1}$ $mW^{-1}$. A fit including the wall loss rate, $k_{loss}$ (Eq. (6), see text) is shown by the blue dashed line and gave $C_{CH3O2}$ = (1.15 ± 0.03) × $10^{-10}$ counts $cm^3$ $molecule^{-1}$ $s^{-1}$ $mW^{-1}$. The close overlap of the two fits shows the wall loss is insignificant and may be ignored.~~ The $C_{CH3O2}$ errors given above represent statistical uncertainties at $1\sigma$ level.

**Table 1**. Average sensitivity factors for the FAGE instrument using the $CH_3O_2$ kinetic decay method under each chamber environment. Examples of these decays can be found in Figure 1 above and in the SI, Figures S3~~2~~ and S4~~3~~, and reported values are typically from an average of 8 decays. All the data were fitted using Eq. (5). The errors given in the table are overall uncertainties (13%) at $1\sigma$ level.

| **Chamber Conditions** | **$C_{CH_3O_2}$ / counts $cm^3$ $molecule^{-1}$ $s^{-1}$ $mW^{-1}$** |
|---|---|
| 80 mbar, He + $O_2$ | (3.83 ± 0.50) × $10^{-9}$ |
| 100 mbar, Air | (2.80 ± 0.37) × $10^{-9}$ |
| 1000 mbar, Air | (1.16 ± 0.15) × $10^{-9}$ |

Table 1 shows the average sensitivity factors obtained fitting Eq. (5) to a typical number of 8 temporal decays of $S_{CH_3O_2}$ under each of the chamber conditions, and example decay traces for the 80 and 100 mbar experiments can be found in the SI, Figs S3~~2~~ and S4~~3~~, respectively. These factors are used for their respective experimental conditions. For the 1000 mbar intercomparison experiments with CRDS, an average of the water vapour photolysis sensitivity factor at 1000 mbar, $C_{CH3O2, H2O}$ = (8.03 ± 1.37) × $10^{-10}$ counts $cm^3$ $molecule^{-1}$ $s^{-1}$ $mW^{-1}$, and the average sensitivity factor obtained from the kinetic decay, $C_{CH3O2, kinetic}$ = (1.16 ± 0.15) × $10^{-9}$ counts $cm^3$ $molecule^{-1}$ $s^{-1}$ $mW^{-1}$ (Table 1), is used, giving $C_{CH3O2, av.}$ = (9.81 ± 2.03) × $10^{-10}$ counts $cm^3$ $molecule^{-1}$ $s^{-1}$ $mW^{-1}$. We make a brief comment regarding the difference in the sensitivity factors $C_{CH3O2, H2O}$ and $C_{CH3O2, kinetic}$, for which the ratio is ~ 0.7, showing a ~30% difference, although the two calibration methods have overlapping error limits at $2\sigma$ level. The kinetic method relies on the rate coefficient $k_{obs}$ for the $CH_3O_2$ self-reaction as recommended by IUPAC (Atkinson et al., 2006), which has a quoted $2\sigma$ uncertainty of 23%. In a separate paper we will present a detailed study of the kinetics of the $CH_3O_2$ self-reaction, and its temperature dependence, and report a revised rate coefficient for this reaction at 298 K.

As the pressure in the FAGE detection cell was 2-3 orders of magnitude lower than the corresponding pressure in HIRAC (*vide supra* in Sect. 2.2) the concentrations of the reagents ($Cl_2$, methane and acetone) were also 2-3 orders of magnitude lower in the fluorescence cells than the reagent concentrations in HIRAC. However, a potential effect of the reagents ($Cl_2$, methane and acetone) on the FAGE sensitivity factor in the HIRAC experiments was investigated. Two different concentrations of $CH_4$ were used in the kinetic method for FAGE calibration at 80 mbar of He + $O_2$ in HIRAC to find practically the same sensitivity factor: (3.80 ± 0.50) × $10^{-9}$ counts $cm^3$ $molecule^{-1}$ $s^{-1}$ $mW^{-1}$ for $2.5 \times 10^{16}$ molecule $cm^{-3}$ $CH_4$ ($2.8 \times 10^{14}$ molecule $cm^{-3}$ in the fluorescence cell) and (3.86 ± 0.50) × $10^{-9}$ counts $cm^3$ $molecule^{-1}$ $s^{-1}$ $mW^{-1}$ for $2.5 \times 10^{17}$ molecule $cm^{-3}$ $CH_4$ ($2.8 \times 10^{15}$ molecule $cm^{-3}$ in the fluorescence cell). As shown in Fig. S1 in the Supplement there is a good agreement between the laser

excitation scans of $CH_3O$ obtained from the $CH_3O_2$ generated in HIRAC using the two methods: acetone photolysis and $Cl_2$ photolysis in the presence of $CH_4$ and $O_2$. In addition, a good agreement has been previously found between the laser excitation spectra of $CH_3O$ generated using the reaction of $CH_4$ with OH (generated by the 254 nm photolysis of water) in the presence of $O_2$ and directly, through the 254 nm photolysis of $CH_3OH$. Therefore, no effect of the used reagents on the laser excitation spectrum of $CH_3O$ was found.

### 2.2.3 FAGE measurements of $CH_3O_2$ concentration gradient across the HIRAC diameter

Measurement of radical gradients across the chamber diameter have been performed previously for $HO_2$ radicals (Onel et al., 2017a), where no gradient was observed until measuring <10 cm from the chamber wall where the signal began to decrease, ultimately by ~16 % at the point at which the FAGE sampling pinhole was level with the chamber walls. To investigate any similar gradient effects for $CH_3O_2$, a steady state concentration of $CH_3O_2$ was generated in the chamber at atmospheric pressure by photolysing $O_3$ in the presence of air and methane:

$$O_3 + h\nu\ (254\ nm) \rightarrow O_2 + O(^1D) \quad \text{(R12)}$$

$$O(^1D) + CH_4 \rightarrow CH_3 + OH \quad \text{(R13)}$$

$$CH_3 + O_2 + M \rightarrow CH_3O_2 + M \quad \text{(R1)}$$

Ozone and methane were present in the chamber at ~$2.5 \times 10^{13}$ molecule $cm^{-3}$ and $2.5 \times 10^{17}$ molecule $cm^{-3}$ respectively. The FAGE inlet was translated across the width of the chamber and the $CH_3O_2$ signal was observed to show no decrease within the ~10% 1σ statistical error of each measurement up until the point at which the pinhole was level with the chamber walls. Moving the instrument further backwards positioned the pinhole inside the ISO-K160 coupling flange and effectively ~4 cm behind the chamber walls where there is likely to be little air movement. This position is analogous to that of the CRDS mirrors, which are recessed into the chamber walls as they mount to the outside of the chamber (see Sect. 2.3). In this position a signal drop of ~14 % was observed, within the statistical error margins of the measurements. A plot of the radical gradient is shown in the Supplementary Information, Figure S54.

### 2.3 CRDS set-up

The optical path of the CRDS spectrometer within the HIRAC chamber is shown in Fig. 2 and is the same spectrometer as used to probe $HO_2$ across the chamber's diameter, and which has been described previously (Onel et al., 2017a).

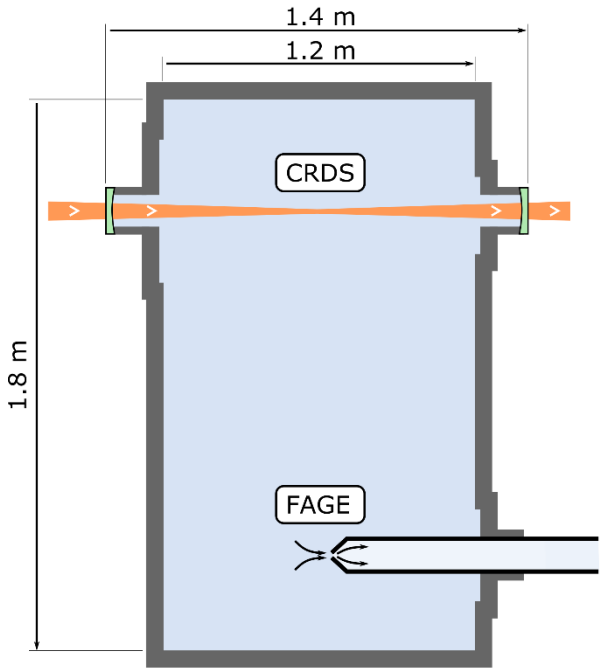


**Figure 2.** Longitudinal (horizontal) section of the HIRAC chamber. The CRDS spectrometer probes the $CH_3O_2$ concentration as an average across the chamber's diameter, while the FAGE instrument probes $CH_3O_2$ in the chamber at a single point close to the centre.

The cavity is formed by two highly reflective 1 in. diameter mirrors (99.999 %, Layertec, curvature radius = 1 m) housed in custom built mounts that allow the mirrors to be tilted slightly whilst maintaining a gas-tight seal. The position of the mirror on the laser injection side is modulated along the cavity axis by a few microns using a piezoelectric transducer at ~10 Hz, with the overall distance between the two mirrors being ~1.4 m. Laser light of ~1.335 μm is generated by a distributed feedback (DFB) fibre pig-tailed diode laser (NTT Electronics, NLK1B5EAAA) held in a butterfly laser diode mount (Thorlabs LM14S2). The electrical current that drives the laser diode and thermoelectric cooler is generated by a Thorlabs ITC502 driver. The DFB is connected to an inline optical isolator (Thorlabs IO-H-1335APC), an acousto-optic modulator (AOM, Gooch & Housego Fibre-Q M040-0.5C8H-3-F2S) and a fibre collimator (Thorlabs CFC-8X-C). The laser light is then guided into the cavity by two silver mirrors (Thorlabs PF10-03-P01). On the detection side of the cavity, light leaking out of the mirror is directed onto another silver mirror that guides the light through a $f$ = 30 mm focusing lens (Thorlabs LA1805-C) onto an InGaAs photodiode (Thorlabs DET10C/M) that is isolated from ambient light by a 1250 nm longpass filter (Thorlabs FELH1250). The photodiode signal is amplified (FEMTO DLPCA-200) and sent to a data acquisition unit (DAQ, National Instruments USB-6361) and to a custom-built comparator that acts as a trigger unit. The comparator compares the amplified photodiode signal with a manually adjustable threshold voltage, and upon reaching a preset threshold the AOM is switched off, stopping the injection of light into the cavity within tens of nanoseconds and initiating a ring-down event. The DAQ is simultaneously triggered and acquires the signal ring-down. The system resets after a set time (typically 5 ms) ready for the next event. The acquired data are processed using a custom made LabView program that fits the ring-down events with an exponential function to extract the ring-down time, $\tau$. Filters are applied to process the ring-down events to exclude potential outliers caused by dust particles passing through the beam and false positives (when the acquisition is triggered by a transient noise spike), so that only legitimate ring-down events are taken into account. The ring-down time can then be converted into the absorption coefficient, $\alpha$:

$$\alpha = \frac{1}{c} \times (1/\tau - 1/\tau_0) \quad (7)$$

where $\tau$ and $\tau_0$ are the ring-down times with and without $CH_3O_2$ radicals present, respectively, and $c$ is the speed of light. $\tau_0$ would be obtained in a typical experiment by recording ring-down events for ~ 1 minute before switching on the photolysis lamps in the chamber. As it is not possible to measure $\tau_0$ and $\tau$ simultaneously, the background was monitored regularly during each experiment by switching off the photolysis lamps and allowing the signal to return to the baseline.

The molecular chlorine delivery did not result in a change in the measured ring-down time. However, delivery of the methane and acetone reagents led to a decrease in the ring-down time indicating that, in the concentrations delivered to the chamber, methane and acetone absorbed in the wavenumber range used in the present work, ~7486–7491 $cm^{-1}$. An absorption coefficient of ~$8 \times 10^{-9}$ $cm^{-1}$ was measured for [acetone] ≈ $9 \times 10^{14}$ molecule $cm^{-3}$ at the typical measurement point of 7487.98 $cm^{-1}$ (*vide infra*). An absorption coefficient in the range (0.7–1.4) × $10^{-8}$ $cm^{-1}$ was determined at 7487.98 $cm^{-1}$ for $CH_4$ in typical concentrations in the FAGE–CRDS intercomparison experiments in the range (1.2–2.5) × $10^{16}$ molecule $cm^{-3}$. The background ring-down time $\tau_0$ (Eq. 7) contained the contributions of the reagents, methane or acetone, and was monitored regularly during the experiments by turning off the chamber lamps (*vide supra*).

The $CH_3O_2$ absorption feature used in these measurements is a band associated with the $A^2A' \leftarrow X^2A''$ electronic transition centred around 7488 $cm^{-1}$, and has been documented in previous work (Faragó et al., 2013, Atkinson and Spillman, 2002, Pushkarsky et al., 2000). There are interfering methane and water vapour lines in this region, and these together with the change in [$CH_3O_2$] during longer (≳ 10~~5~~ min) scanning times did not allow us to generate a continuous, high resolution scan across the $CH_3O_2$ transition. Instead, as shown in Fig. 3, the absorption spectrum was mapped out as a series of point measurements at fixed wavelengths, normalised by the absorption at the optimum measurement point, 7487.98 $cm^{-1}$ ~~(rounded to 7488 $cm^{-1}$ henceforth)~~, where the absorption feature is sufficiently strong and furthest in wavelength from interfering methane absorption lines and where the $CH_3O_2$ cross section was determined (Sect. 3.2). The absorption coefficient of $CH_4$ was about 7 times lower at 7487.98 $cm^{-1}$ than at 7489.16 $cm^{-1}$, i.e. at the peak of the $CH_3O_2$ spectral feature where Fittschen (2019) reported $\sigma_{CH3O2}$. Therefore, 7487.98 $cm^{-1}$ (rounded to 7488 $cm^{-1}$ henceforth) was chosen as the measurement point instead of the value of 7489.16 $cm^{-1}$ used by Fittschen (2019). Each datum~~a~~ point in Fig. 3 was obtained by measuring the absorption coefficient, $\alpha_{7488\ cm^{-1}}$, and the baseline (lamps on, then off) at 7488 $cm^{-1}$ followed by measuring $\alpha_{CH3O2}$ and baseline at another wavelength on the absorption feature and then reverting to measuring at 7488 $cm^{-1}$ again. This pattern was repeated multiple times for different wavelengths to build up an absorption feature, with all data points normalised to $\alpha_{7488\ cm^{-1}}$ and then multiplied by the $CH_3O_2$ cross section at 7488 $cm^{-1}$ (Sect. 3.2) to obtain the absorption spectrum shown in Fig. 3. The method was used to measure the $CH_3O_2$ absorption spectrum under each of the three experimental conditions detailed in Sect. 2.1: 80 mbar (He + $O_2$) and 100 mbar and 1000 mbar of synthetic air.

## 3 Results

### 3.1 $CH_3O_2$ absorption spectrum and comparison with the literature

Figure 3 shows that the relatively broad absorption feature obtained in this work in the range from ~7486 to 7491 $cm^{-1}$ is almost the same at 80 mbar He:$O_2$ = 3:1 and at 100 and 1000 mbar of synthetic air. As shown in Fig. 3, the spectrum found in this work agrees well with the general shape of the $CH_3O_2$ spectrum measured by Faragó et al. (2013) at 67 mbar He:$O_2$ ~ 1:1 but scaled to reflect the very recent update to the absolute absorption cross-section reported by Fittschen (2019) which gave $\sigma_{7489\ cm^{-1}}$ = $2.2 \times 10^{-20}$ $cm^2$ $molecule^{-1}$. The peaks at the top of the spectral feature reported by Faragó et al. (2013) are not reproduced in this work owing to the method of generating the spectrum~~, which did not allow for a high resolution~~ (Sect. 2.3)~~, and a potential small difference in wavelength compared to λ in the spectrum reported by Faragó et al. (2013)~~. Previously Pushkarsky et al. (2000) measured the $CH_3O_2$ absorption spectrum over a larger wavenumber range (7300–7700 $cm^{-1}$) where the $\nu_{12}$ transition is located at 7488 $cm^{-1}$ in agreement with this work. In addition, if the $CH_3O_2$ spectrum at 27 mbar $N_2$:$O_2$ =

4:1 reported by Atkinson and Spillman (2002) were shifted by ~2 $cm^{-1}$ toward higher wavenumbers compared to this work and the study of Faragó et al. (2013), the shape of the $\nu_{12}$ band from Atkinson and Spillman is in agreement with the results shown in Fig. 3.

The similarity of the results at 80 mbar $He:O_2$ = 3:1 and at 100 and 1000 mbar of air reported in this work and their agreement with the previous measurements performed at relatively low pressures (Fittschen, 2019; Faragó et al., 2013; Atkinson and Spillman, 2002; Pushkarsky et al., 2000) can be explained by an overlap of several individual absorption lines resulting in a spectral structure in the range from ~7486 to 7491 $cm^{-1}$ with practically no pressure dependence observed between ~30–1000 mbar. Therefore, it can be assumed that the absorption cross section at 7488 $cm^{-1}$, $\sigma$(7488 $cm^{-1}$), is the same under the conditions used in this work, i.e. at 80 mbar of He and $O_2$ and at 100 and 1000 mbar of air.

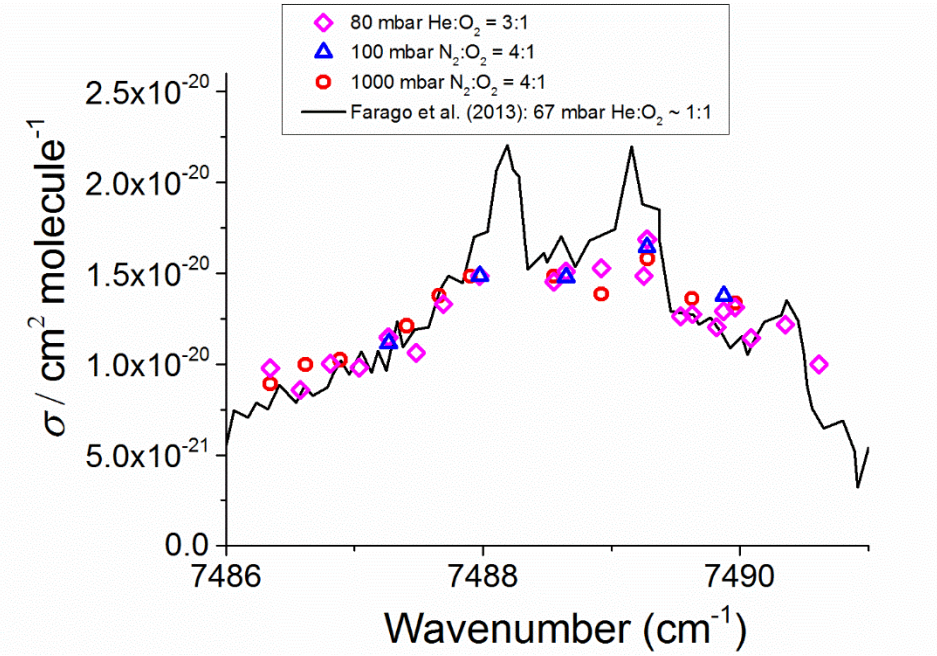


**Figure 3**. $CH_3O_2$ absorption spectrum at 295 K. The measured absorption spectrum scaled to the absolute cross section determined at 7488 $cm^{-1}$ using the kinetics of the $CH_3O_2$ decay monitored using CRDS (Sect. 3.2 below). The black line represents the $CH_3O_2$ spectrum measured by Faragó et al. (2013) at 67 mbar $He:O_2$ ~ 1:1 but with the absolute cross-section scaled to reflect the recent update reported by Fittschen (2019) giving $\sigma_{7489\ cm^{-1}} = 2.2 \times 10^{-20}$ $cm^2$ $molecule^{-1}$.

### 3.2 Determination of the absorption cross section of $CH_3O_2$ at 7488 $cm^{-1}$

The kinetics of the $CH_3O_2$ temporal decay by its self-reaction (Reaction R5) were used to determine the absorption cross section of $CH_3O_2$ at 7488 $cm^{-1}$, $\sigma$(7488 $cm^{-1}$). Note that the cross-section used is not the more standard integrated cross-section used by HITRAN and other spectral databases. $CH_3O_2$ radicals were generated by using $CH_4/Cl_2$/synthetic air mixtures (Sect. 2.1) with the chamber UV lamps switched on to generate Cl atoms (R6). By extinguishing the UV lamps, $CH_3O_2$ radicals were removed by self-reaction and wall loss. Figure 4 shows an example of a kinetic decay obtained at 100 mbar $N_2:O_2$ = 4:1 using CRDS. The experimental data were fitted by using two functions described by Eqs. (8) and (9), which are closely related to Eqs. (4) and (5) used in the analysis of the $CH_3O_2$ decays measured using FAGE. Equation (8) assumes that the wall loss of $CH_3O_2$ is negligible and hence the removal of $CH_3O_2$ can be described by the integrated second–order rate law equation, leading to:

$$\alpha_t = \left(\frac{1}{\alpha_0} + \frac{2 \cdot k_{obs} \cdot \Delta t (t - t_0)}{\sigma(7488\ cm^{-1})}\right)^{-1}, \quad (8)$$

where $\alpha_t$ is the $CH_3O_2$ absorption coefficient at 7488 $cm^{-1}$ and at time $t$, $\alpha_0$ is the absorption coefficient at time zero of the reaction when the lamps are switched off, $t_0$, $\Delta t = t - t_0$ and $k_{obs}$ is the observed rate coefficient of the self-reaction at 298 K, $k_{obs} = (4.8 \pm 0.6) \times 10^{-13}$ $cm^3$ $molecule^{-1}$ $s^{-1}$ (Atkinson et al., 2006).

For completeness, Equation (9) includes the $CH_3O_2$ wall loss as a first-order process, leading to:

$$\alpha_t = \left( \left( \frac{1}{\alpha_0} + \frac{2 \cdot k_{obs.}}{k_{loss} \cdot \sigma(7488\ cm^{-1})} \right) \times \exp(k_{loss} \Delta t) - \left( \frac{2 \cdot k_{obs.}}{k_{loss} \cdot \sigma(7488\ cm^{-1})} \right) \right)^{-1}, \quad (9)$$

where $k_{loss}$ is the rate coefficient describing the $CH_3O_2$ wall loss (Onel et al., 2017a).

Figure 4 shows that the fits given by Eqs. (8) and (9) to the data overlap over all of the temporal $CH_3O_2$ decay and the values of $\sigma(7488\ cm^{-1})$ extracted by the two fits are in a very good agreement: $(1.47 \pm 0.07) \times 10^{-20}$ $cm^2$ $molecule^{-1}$ (Eq. (8)) and $(1.50 \pm 0.07) \times 10^{-20}$ $cm^2$ $molecule^{-1}$ (Eq. (9)), where the quoted errors are statistical uncertainties. The values extracted for $k_{loss}$ by fitting Eq. (9) to the CRDS data were small and similar to the values obtained by fitting Eq. (6) to the kinetic decays monitored by FAGE. An upper limit of ~ $1 \times 10^{-5}$ $s^{-1}$ was obtained for $k_{loss}$ in both FAGE and CRDS measurements, showing that wall losses are negligible. From fitting Eq. (8) to the temporal decays obtained at 100 mbar of synthetic air, an averaged value of $(1.51 \pm 0.19) \times 10^{-20}$ $cm^2$ $molecule^{-1}$ was obtained, where the error represents 1σ overall uncertainty (13%). Fitting Eq. (8) to the data at 80 mbar $He:O_2$ = 3:1 (Fig. S6), gave an average value of $\sigma(7488\ cm^{-1}) = (1.46 \pm 0.17) \times 10^{-20}$ $cm^2$ $molecule^{-1}$ (1σ overall uncertainty), in very good agreement with the value at 100 mbar of air. The average of the results at 80 mbar $He:O_2$ = 3:1 and 100 mbar of air, $1.49 \times 10^{-20}$ $cm^2$ $molecule^{-1}$, is in excellent agreement with the determination of Atkinson and Spillman (2002): $\sigma_{max}(\nu_{12}) = (1.5 \pm 0.8) \times 10^{-20}$ $cm^2$ $molecule^{-1}$ and consistent with the estimation of ~$1.0 \times 10^{-20}$ $cm^2$ $molecule^{-1}$ for $\sigma_{max}(\nu_{12})$ obtained using the $CH_3O_2$ spectrum reported by Pushkarsky et al. (2000). To enable a comparison at 7487.98 $cm^{-1}$ with the very recent measurement of Fittschen (2019), who found $2.20 \times 10^{-20}$ $cm^2$ $molecule^{-1}$ at 7489.16 $cm^{-1}$, $\sigma(7487.98\ cm^{-1}) = 1.49 \times 10^{-20}$ $cm^2$ $molecule^{-1}$ obtained in this work was multiplied by the $\sigma(7489.16\ cm^{-1}):\sigma(7487.98\ cm^{-1})$ ratio obtained by using the high resolution spectrum reported by Faragó et al. (2013) (Fig. 3). The obtained value, $\sigma(7489.16\ cm^{-1}) = (1.9 \pm 0.3) \times 10^{-20}$ $cm^2$ $molecule^{-1}$ is in reasonable agreement with the result of Fittschen (2019), $\sigma(7489.16\ cm^{-1}) = 2.2 \times 10^{-20}$ $cm^2$ $molecule^{-1}$.

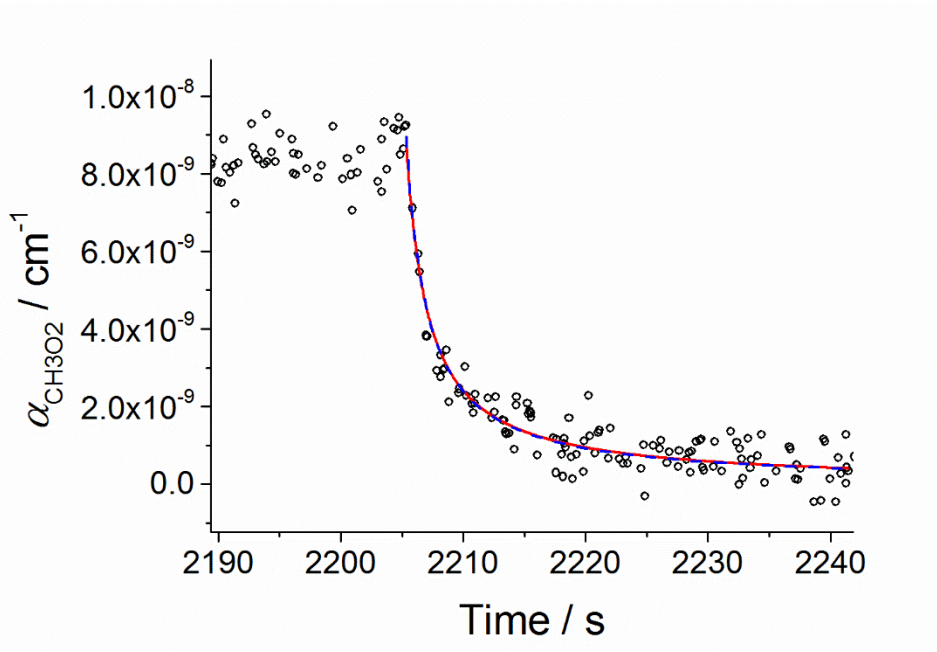

**Figure 4.** Second -order decay of the $CH_3O_2$ absorption coefficient at 7488 $cm^{-1}$ monitored by CRDS. Experiment carried out at 295 K and 100 mbar of synthetic air; $[CH_4]_0 = 2.4 \times 10^{16}$ molecule $cm^{-3}$ and $[Cl_2]_0 = 1.0 \times 10^{15}$ molecule $cm^{-3}$. At time 2205 s the photolysis lamps were turned off (time $t_0$). Fitting Eq. (8) to the data (red line) gave $\sigma(7488\ cm^{-1}) = (1.47 \pm 0.07) \times 10^{-20}$ $cm^2$ $molecule^{-1}$. A fit including the wall loss rate, $k_{loss}$ (Eq. (9)) is shown by the blue dashed line and resulted in $\sigma(7488\ cm^{-1}) = (1.50 \pm 0.07) \times 10^{-20}$ $cm^2$ $molecule^{-1}$. The error limits are statistical errors at $1\sigma$ level.

### 3.3 Determination of the CRDS limit of detection

The CRDS limit of detection (*LOD*) has been computed using plots of the square root of the Allan-Werle variance ~~Allan-Werle deviation plots~~ (Werle et al., 1993;Onel et al., 2017a) obtained by continuously recording single ring-down events for 1–2 hr after delivering either acetone or methane in typical concentrations to the chamber filled with the bath gas ($He:O_2$ = 3:1 at 80 mbar and synthetic air at 100 and 1000 mbar, respectively). The square root of the Allan-Werle variance, here referred to as t~~T~~he Allan-Werle deviation, $\sigma_A(n)$, gives an estimate of the error, $\delta\alpha$, between successively measured absorption coefficients for a given averaging size *n*. For a signal-to-noise ratio (*S*/*N*) of 2, the limit of detection for $CH_3O_2$ was determined as $LOD_{CH3O2} = (2\delta\alpha_{min})/\sigma_{CH3O2}$, where $\sigma_{CH3O2} = 1.49 \times 10^{-20}$ $cm^2$ $molecule^{-1}$ is the $CH_3O_2$ cross section at 7488 $cm^{-1}$, and is shown in Table 2. The optimum CRDS sensitivity under all conditions is achieved averaging ~500 ring-down events, requiring ~77 s at an acquisition rate of 6.5 Hz on average, with an example shown in Fig. 5.

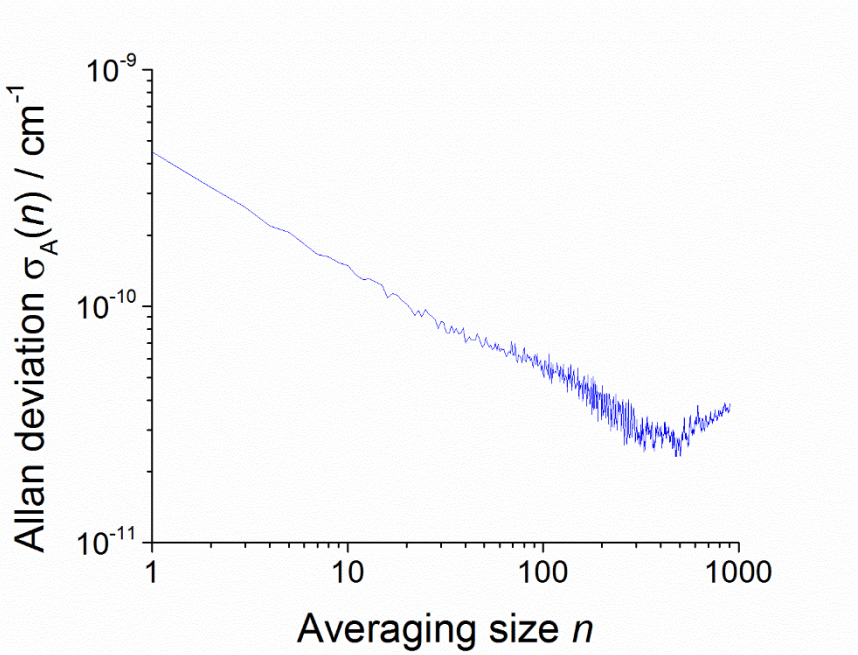


**Figure 5.** An example of the Allan-Werle deviation plot (the plot of the square root of the Allan-Werle variance) of the absorption coefficient at 7488 $cm^{-1}$ in the absence of $CH_3O_2$ and the presence of a typical acetone concentration of $8.8 \times 10^{14}$ molecule $cm^{-3}$ at 1000 mbar against the number of ring-down events averaged, *n*. For *S*/*N* = 2 the minimum detectable absorption coefficient for a single ring-down measurement is $4.5 \times 10^{-10}$ $cm^{-1}$, which decreases to a minimum of $2.89 \times 10^{-11}$ $cm^{-1}$ after *n* = 500 (requiring 77 s at an acquisition rate of 6.5 Hz).

As the filter (FELH1250 Thorlabs, cut-off wavelength: 1250 nm) used to cut-off the laboratory visible light from the background of the CRDS measurements allowed some of the 254 nm light generated by the HIRAC lamps to be transmitted and then detected by the InGaAS photodiode detector, the CRDS sensitivity was worse in the experiments using acetone/$O_2$/254 nm lamps as a source of $CH_3O_2$ compared to the experiments using $Cl_2/CH_4/O_2$/UV black lamps to generate $CH_3O_2$. Therefore, separate Allan-Werle deviation plots were constructed using measurements of single ring-down events after filling HIRAC with the bath gas and turning the 254 nm lamps on. Then, the composite error, calculated as the sum in quadrature of $\delta\alpha$ obtained in the presence of acetone and $\delta\alpha$ determined in the absence of acetone but keeping the 254 nm lamps turned on, was used to determine the *LOD* of CRDS in the acetone/$O_2$/254 nm experiments (Table 2). The composite

*LOD*(acetone/$O_2$/254 nm lamps) was on average ~55% greater than the *LOD* determined with the UV lamps off and in the absence of acetone, *LOD*(bath gas); and on average *LOD*($Cl_2$/$CH_4$/$O_2$/UV black lamps) was ~40% higher than *LOD*(bath gas)

**Table 2**. CRDS detection limits for $CH_3O_2$ calculated at 80 mbar He:$O_2$ = 3:1 and 100 mbar and 1000 mbar of synthetic air for single ring-down measurements ($\Delta t$ = 0.15 s), the optimum averaging time obtained from Allan-Werle deviation plot (Fig. 5 shows an example), $\Delta t_{opt.}$ (77 s under all experimental conditions) and $\Delta t$ = 60 s.

| **Bath gas** | $p_{HIRAC}$ / **mbar** | **Reagent delivered to HIRAC** | $LOD_{CH3O2}$ / $10^9$ molecule cm$^{-3}$ | | |
|---|---|---|---|---|---|
| | | | $\Delta t$ = 0.15 s | $\Delta t$ = 60 s | $\Delta t_{opt}$ = 77 s. |
| He:$O_2$ = 3:1 | 80 | acetone[a] | 120 | 7.5 | 6.4 |
| Air | 100 | acetone[a] | 133 | 8.6 | 6.8 |
| | | methane[b] | 78 | 6.0 | 5.4 |
| Air | 1000 | acetone[a] | 147 | 7.3 | 6.1 |

[a] using the composite error calculated as the sum in quadrature of $\delta\alpha$ obtained using a typical concentration of acetone, 8.8 × $10^{14}$ molecule cm$^{-3}$, and $\delta\alpha$ determined in the absence of acetone but keeping the 254 nm lamps turned on during all measurement.
[b] [$CH_4$] = 2.4 × $10^{16}$ molecule cm$^{-3}$.

As the daytime concentrations of $CH_3O_2$ have been calculated using an atmospheric box-model to peak at ~$10^7$–$10^8$ molecule cm$^{-3}$ (Whalley et al., 2010;Whalley et al., 2011;Whalley et al., 2018), the current CRDS sensitivity is insufficient for the detection of ambient [$CH_3O_2$]. The typical concentrations of $CH_4$ and acetone in ambient air are orders of magnitude lower than [$CH_4$] and [$(CH_3)_2CO$] used in the HIRAC experiments. However, water vapour, which is present in the atmosphere in much larger concentrations (typically ~$10^{17}$ molecule cm$^{-3}$) than in HIRAC for these experiments (~ $10^{13}$ – $10^{14}$ molecule cm$^{-3}$), will significantly absorb in this wavelength region and contribute towards the background of the measurements. The limits of detection shown in Table 2 allow for HIRAC measurements of [$CH_3O_2$] $\gtrapprox$ $10^{10}$ molecule cm$^{-3}$ in steady-state (where averaging times of ~60 s can be used) under all conditions used, and kinetic measurements of [$CH_3O_2$] $\gtrapprox$ $10^{11}$ molecule cm$^{-3}$ with the present instrument resolution time (0.15 s) at 80 mbar He:$O_2$ = 3:1 and 100 mbar of air.

The relatively long ring-down times achieved here require the lasers to be blocked for several ms during which the full exponential ring-down is measured. This imposes an upper limit to the ring-down rate. The achieved rate is significantly smaller (6.5 Hz on average) for the following reasons. The width of the resonances of the optical cavity is of the order of 1 kHz, much narrower than the laser linewidth. This makes the injection of light into the cavity inefficient. Reducing the laser linewidth, e.g. with optical feedback techniques, could significantly increase the injection efficiency and the ring-down rate. Moreover, the resonance frequencies jitter and drift due to the unavoidable vibrations associated with the operation of the HIRAC chamber. The cavity length was actively modulated in order to repeatedly force coincidence of laser and resonance frequency. Due to the poor injection efficiency mentioned above, however, not every coincidence resulted in a ring-down event. Furthermore, a significant fraction of the ring-down events has to be discarded because of the passage of dust particles, moved around by the fans within the chamber, through the cavity axis.

The use of an additional optical filter to cut-off the 254 nm light from the background of the CRDS measurements is expected to improve the CRDS sensitivity if the 254 nm lamps are used in HIRAC. The CRDS sensitivity could be further improved by mounting the cavity mirrors along the HIRAC length, which would result in a cavity of about 2 m length containing $CH_3O_2$ radicals, and, hence ~~by increasing the frequency of the ring- down events and using a cavity length~~ above the current 1.4 m length. Although the origin band centred at 7388 cm$^{-1}$ is about three times stronger than the methyl torsional

band at 7488 $cm^{-1}$ (Pushkarsky et al., 2000;Chung et al., 2007), the latter was targeted because absorption due to water vapour is between one and three orders of magnitude weaker there (assuming 1% v/v, atmospheric pressure) (Gordon et al., 2017).

### 3.4 Intercomparison of CRDS and FAGE $CH_3O_2$ measurements

All the intercomparison measurements have been performed at 7488 $cm^{-1}$, where the $CH_3O_2$ cross section was determined using CRDS (Sect. 3.2). For the measurements at 80 mbar He:$O_2$ (3:1) and 100 mbar $N_2$:$O_2$ (4:1), $CH_3O_2$ was generated either from the photolysis of acetone at 254 nm in the presence of $O_2$ or from the photolysis of $Cl_2$ using UV black lamps in the presence of $CH_4$/$O_2$. At 1000 mbar of synthetic air, the overlap of the methane absorption lines due to the pressure broadening resulted in a significant $CH_4$ absorption over the range from 7486–7491 $cm^{-1}$ in the background of the $CH_3O_2$ measurements. Therefore, all the measurements at 1000 mbar have been carried out using the photolysis of acetone/$O_2$ at 254 nm. The data recorded by CRDS using acetone/$O_2$ were more scattered than the CRDS data recorded using $Cl_2$/$CH_4$/$O_2$ for the reasons discussed above (see Figs. 6a and 8a in comparison with Fig. 7a) and were the main contributors to the scatter on $[CH_3O_2]_{CRDS}$ in the correlation plots (Figs. 6b, 7b and 8b below). There was less signal noise present in the FAGE measurements, where the most significant source of noise is the shot noise (Poisson noise), which increases with the number of photons counted by the detector (Figs. 1, S~~2~~3 and S4~~3~~) and results in a scatter on the FAGE data growing with $[CH_3O_2]$ in Figs 6a, 7a and 8a.

As the acquisition rate of CRDS (6.5 Hz in average) differed compared to the FAGE acquisition rate (in the range 1–10 Hz) the comparison data were averaged to enable comparison of $[CH_3O_2]$ by the two instruments at the same moments of time. The averaging interval of time was chosen in the range 3–5 s depending on the comparison measurement to average at least 10 ring-down events over each time interval as the CRDS data were filtered to exclude outliers caused by dust particles passing through the light beam trapped in the optical cavity and the number of encountered 'dust events' varied from one experiment to another.

$CH_3O_2$ was generated over a range of concentrations, 2–26 × $10^{10}$ molecule $cm^{-3}$ at 80 mbar of He + $O_2$ mixture, 2–60 × $10^{10}$ molecule $cm^{-3}$ at 100 mbar of synthetic air and 2–30 × $10^{10}$ molecule $cm^{-3}$ at 1000 mbar of synthetic air. The comparison involved both periods with lamps on where the concentration of $CH_3O_2$ was changing slowly, and where the lamps were turned off and the rapid decay of $CH_3O_2$ was observed. Figures 6a, 7a and 8a show examples of time-resolved $CH_3O_2$ concentrations where the lamps were turned on and off. CRDS absorption coefficients were converted into concentrations using the absorption cross section determined by studying the second-order recombination kinetics, $\sigma$(7488 $cm^{-1}$) = (1.49 ± 0.19) × $10^{-20}$ $cm^2$ $molecule^{-1}$ (Sect. 3.2). The FAGE signals were converted into $[CH_3O_2]$ using the sensitivity factor derived from the analysis of the temporal decays of $CH_3O_2$ at 80 mbar of He + $O_2$ mixture and 100 mbar of air, (3.83 ± 0.50) × $10^{-9}$ counts $cm^3$ $molecule^{-1}$ $s^{-1}$ $mW^{-1}$ and (2.80 ± 0.37) × $10^{-9}$ counts $cm^3$ $molecule^{-1}$ $s^{-1}$ $mW^{-1}$, respectively. The data in the correlation plots of the $CH_3O_2$ concentrations determined by FAGE (*y*-axis) and CRDS (*x*-axis) (Figs. 6b, 7b and 8b) were fitted using an orthogonal distance linear regression fit (Boggs et al., 1987), which accounts for errors in both the *y*- and *x*-directions. The gradient of the correlation plot of the $CH_3O_2$ concentrations determined by FAGE (*y*-axis) and CRDS (*x*-axis) at 80 mbar of He + $O_2$ (Fig. 6b) is 1.03 ± 0.05, showing an overall level of agreement within 3%. The gradient of the correlation plot of the $CH_3O_2$ concentrations determined by FAGE (*y*-axis) and CRDS (*x*-axis) at 100 mbar of air (Fig. 7b) is 0.95 ± 0.02, showing an overall level of agreement within 5%.

At 1000 mbar of air, the FAGE signal observed in HIRAC could be calibrated in one of two ways, either via the photolysis of water vapour to generate OH followed by reaction with $CH_4$ to form $CH_3O_2$, or via the kinetic analysis of second order temporal decays of $CH_3O_2$. The conversion of the FAGE signals into $[CH_3O_2]$ at 1000 mbar air for the intercomparison with CRDS shown in Figs. 8a and 8b was based on the average of the results of the water vapour calibration method and the kinetic decay calibration method, which gives $\overline{C}_{CH_3O_2}$ = (9.81 ± 2.03) × $10^{-10}$ counts $cm^3$ $molecule^{-1}$ $s^{-1}$ $mW^{-1}$ (Sect. 2.2.2)). The gradient of the overall correlation plot (Fig. 8b) using $\overline{C}_{CH_3O_2}$ is 1.09 ± 0.06, showing agreement to within 9%. Figure S7~~6~~ in

the Supplementary Information shows separately the two correlation plots obtained using the sensitivities from the two methods of calibration for FAGE: $C_{CH_3O_2}$ = (8.03 ± 1.37) × $10^{-10}$ counts $cm^3$ $molecule^{-1}$ $s^{-1}$ $mW^{-1}$ (water vapour calibration method) and $C_{CH_3O_2}$ = (1.16 ± 0.15) × $10^{-9}$ counts $cm^3$ $molecule^{-1}$ $s^{-1}$ $mW^{-1}$ (second order kinetic decay method). The gradients of the two linear fits are: 1.35 ± 0.07 (water vapour calibration) and 0.92 ± 0.05 (kinetic method of calibration). Therefore, a significantly better agreement (within 8%) was obtained by using the kinetic method for the calibration of FAGE compared with using the water vapour method for calibration of FAGE (35% agreement). Better agreement is expected when using the kinetic method to calibrate FAGE, as this is the same method used to determine the absorption cross section and hence calibrate ~~of~~ the CRDS method, and the intercomparison is not affected by~~subject to~~ any error in the rate coefficient, $k_{obs}$, for the $CH_3O_2$ self-reaction. We consider that the main contribution to the discrepancy in $C_{CH3O2}$ values obtained by the two methods of calibration derives from an overestimation of the reported value of the observed rate coefficient for the $CH_3O_2$ self-reaction, $k_{obs}$ = (4.8 ± 0.6) × $10^{-13}$ $molecule^{-1}$ $cm^3$ $s^{-1}$ ($1\sigma$ error) at 298 K (Atkinson et al., 2006). In a subsequent paper we will report a revised $k_{obs}$, which will bring ~~into agreement~~ the two methods of calibration into agreement.

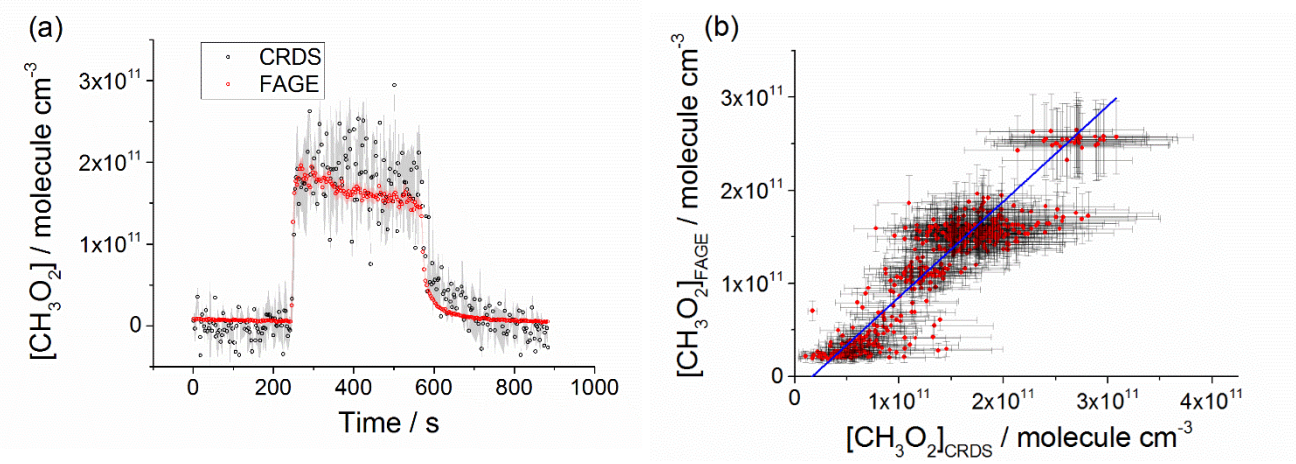


**Figure 6**. (a) Comparison of $CH_3O_2$ measurement at 80 mbar He:$O_2$ (3:1) where the lamps were turned on at $t$ ~ 250 s for ~ 5 min to generate $CH_3O_2$ and then turned off again. The measurement by FAGE is shown in red and the measurement by CRDS is plotted in black. $CH_3O_2$ radicals were generated using the 254 nm photolysis of $(CH_3)_2CO$ (8.8 × $10^{14}$ molecule $cm^{-3}$). The $1\sigma$ statistical errors generated by the data averaging are shown as grey (CRDS) and red (FAGE) shadows. (b) Correlation plot at 80 mbar He:$O_2$ (3:1) combining the data obtained using acetone/$O_2$/254 nm lamps with the data generated using $Cl_2$/$CH_4$/$O_2$/UV black lamps. $[CH_3O_2]$ measured by FAGE is plotted against $[CH_3O_2]$ measured by CRDS. The linear fit to the data generates a gradient of 1.03 ± 0.05 and an intercept of (-1.7 ± 0.5) × $10^{10}$ molecule $cm^{-3}$. The linear fits were generated using the orthogonal distance regression algorithm; fit errors at $2\sigma$ level. In both panels $[CH_3O_2]_{FAGE}$ was determined using a calibration factor of 3.83 × $10^{-9}$ counts $cm^3$ $molecule^{-1}$ $s^{-1}$ $mW^{-1}$ and $[CH_3O_2]_{CRDS}$ was calculated using a cross section of 1.49 × $10^{-20}$ $cm^2$ $molecule^{-1}$. Each point is a value averaged over~~Each point is an averaged value over~~ 3 s.

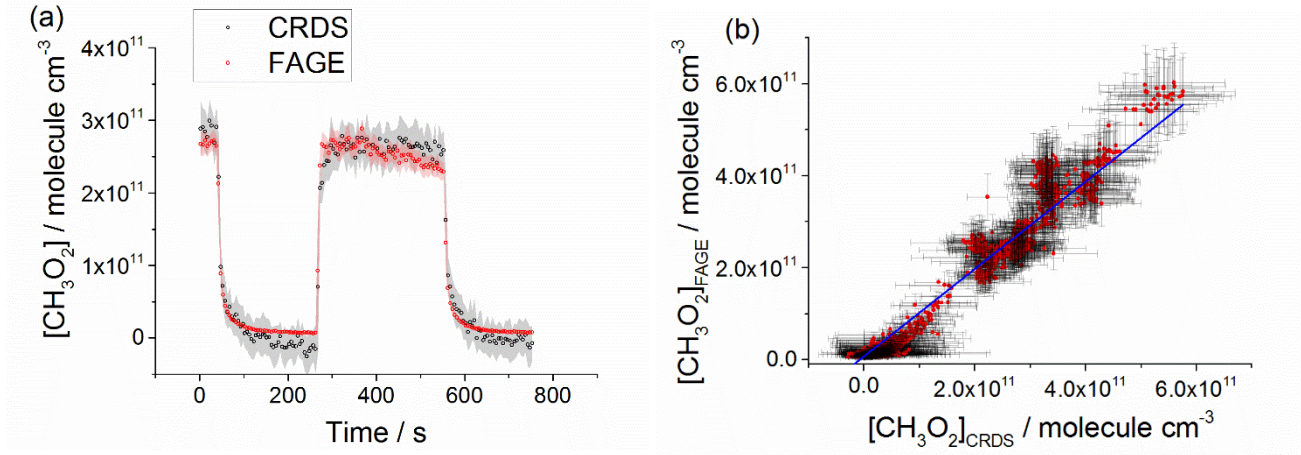


**Figure 7**. Comparison of $CH_3O_2$ measurement (a) and the correlation plot at 100 mbar $N_2$:$O_2$ (4:1) (b). In both figures $[CH_3O_2]_{FAGE}$ was computed using a calibration factor of $2.80 \times 10^{-9}$ counts $cm^3$ $molecule^{-1}$ $s^{-1}$ $mW^{-1}$ and $[CH_3O_2]_{CRDS}$ was determined using a cross section of $1.49 \times 10^{-20}$ $cm^2$ $molecule^{-1}$. ~~Each point is an averaged value over~~ Each point is a value averaged over 5 s. Figure (a) shows the measurement by FAGE (red) and the measurement by CRDS (black) where the $CH_3O_2$ radicals were generated by the photolysis of $Cl_2$ ($2.5 \times 10^{15}$ molecule $cm^{-3}$) in the presence of $CH_4$ ($2.4 \times 10^{16}$ molecule $cm^{-3}$) and $O_2$. The UV black lamps were alternately switched on and off: the lamps were turned off at $t \sim 40$ s and then turned on at $t \sim 250$ s for ~ 5 min before being switched off again. The $1\sigma$ statistical errors generated by the data averaging are shown as grey (CRDS) and red (FAGE) shadows. Figure (b) combines the data obtained using acetone/$O_2$/254 nm lamps with the data generated using $Cl_2$/$CH_4$/$O_2$/UV black lamps. $[CH_3O_2]$ measured by FAGE is plotted versus $[CH_3O_2]$ measured by CRDS. The linear fit to the data is obtained using the orthogonal distance regression algorithm and results in a gradient of 0.95 ± 0.02 and an intercept of $(7.0 \pm 0.4) \times 10^9$ molecule $cm^{-3}$; fit errors given at $2\sigma$ level.

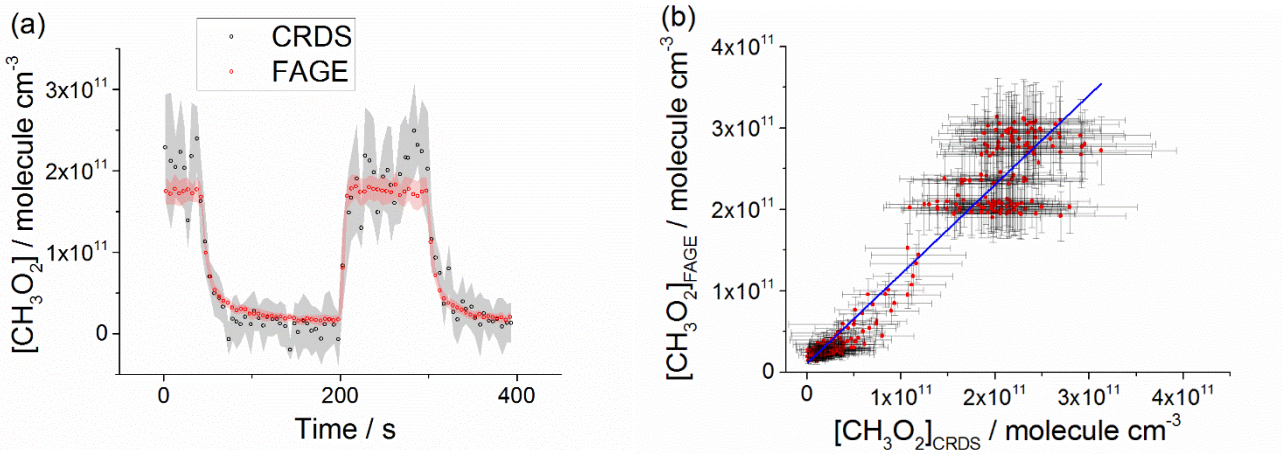


**Figure 8**. (a) Comparison of $CH_3O_2$ measurement at 1000 mbar of synthetic air where the lamps were turned off at $t \sim 40$ s and then on at $t \sim 200$ s for ~ 2 min before being switched off again. The measurement by FAGE is shown in red and the measurement by CRDS is plotted in black. $CH_3O_2$ radicals were generated using the 254 nm photolysis of $(CH_3)_2CO$ ($8.8 \times 10^{14}$ molecule $cm^{-3}$). The $1\sigma$ statistical errors generated by the data averaging are shown as grey (CRDS) and red (FAGE) shadows. (b) Correlation plot of all the data generated at 1000 mbar of air. $[CH_3O_2]$ measured by FAGE is plotted against $[CH_3O_2]$ measured by CRDS. The linear fit to the data is generated using the orthogonal distance regression algorithm and results in a gradient of 1.09 ± 0.06 and an intercept of $(1.1 \pm 0.3) \times 10^{10}$ molecule $cm^{-3}$; fit errors given at $2\sigma$ level. In both panels $[CH_3O_2]_{FAGE}$ was determined using a calibration factor of $9.81 \times 10^{-10}$ counts $cm^3$ $molecule^{-1}$ $s^{-1}$ $mW^{-1}$ and $[CH_3O_2]_{CRDS}$ was calculated using a cross section of $1.49 \times 10^{-20}$ $cm^2$ $molecule^{-1}$. ~~Each point is an averaged value over~~ Each point is a value averaged over 5 s.

## 4 Conclusions

An intercomparison between the recently developed indirect method for the measurement of the $CH_3O_2$ radicals using Fluorescence Assay by Gas Expansion (FAGE) (Onel et al., 2017b) and the direct Cavity Ring-Down Spectroscopy (CRDS)

method has been performed within the Leeds Highly Instrumented Reactor for Atmospheric Chemistry (HIRAC). CRDS detected $CH_3O_2$ by using the $A \leftarrow X$ ($\nu_{12}$) electronic transition at 7488 $cm^{-1}$. The $CH_3O_2$ radical was generated from the photolysis of mixtures of either $Cl_2/CH_4/O_2$ or acetone//$O_2$ at room temperature and three total pressures, 80 mbar of He:$O_2$ = 3:1 and 100 and 1000 mbar of $N_2$:$O_2$ = 4:1, and was measured simultaneously using the two methods.

At all pressures FAGE was calibrated using the kinetics of the $CH_3O_2$ second -order decay by self–reaction. At 1000 mbar the conventional 185 nm photolysis of water vapour in the presence of excess of $CH_4$ and $O_2$ was used to calibrate FAGE in addition to the kinetic method. The two calibration methods have overlapping error limits at $2\sigma$ level (34% for the water vapour photolysis method and 26% for the kinetic method) as it has been found previously (Onel et al., 2017b). The difference between $C_{CH_3O_2}$(water vapour method) and $C_{CH_3O_2}$(kinetic method) has been discussed in detail previously (Onel et al., 2017b). In the case of $HO_2$, a very good agreement (difference within 8%) between $C_{HO_2}$(water vapour method) and $C_{HO_2}$(kinetic method) was obtained previously (Onel et al., 2017a;Winiberg et al., 2015), which suggests that the production of OH and $HO_2$ from the photolysis of water vapour in air can be quantified robustly. We consider it unlikely that there is a significant error in the fraction of OH which is converted to $CH_3O_2$ upon the addition of methane. We consider instead that the discrepancy between the two calibration methods is due to an overestimation of the reported value of $k_{obs}$ for the $CH_3O_2$ self-reaction (Atkinson et al., 2006); the two methods of calibrations agree if $k_{obs}$ is reduced by 25–30%, which is close to the reported $2\sigma$ uncertainty in the rate coefficient (Atkinson et al., 2006). The average value of the sensitivity factor obtained from the two calibration methods, $\overline{C}_{CH_3O_2}$ = (9.81 ± 2.03) × $10^{-10}$ counts $cm^3$ $molecule^{-1}$ $s^{-1}$ $mW^{-1}$, corresponds to a limit of detection (*LOD*) for $CH_3O_2$ of 1.18 × $10^8$ molecule $cm^{-3}$ for a *S*/*N* of 2 and 60 s averaging period. The FAGE sensitivity factor increased by ~3 times by decreasing the pressure in the FAGE detection cell (from 3.3 mbar, corresponding to a total HIRAC pressure of 1000, to 0.9 mbar, corresponding to a total chamber pressure of 100 or 80 mbar ~~to 0.9 mbar corresponding to a total HIRAC pressure of 1000 and 100 or 80 mbar, respectively~~).

The $CH_3O_2$ absorption cross section at 7488 $cm^{-1}$ at 100 mbar of air and 80 mbar of He:$O_2$ = 3:1 was determined using the kinetics of the $CH_3O_2$ second -order decays: $\sigma_{CH3O2}$ = (1.49 ± 0.19) × $10^{-20}$ $cm^2$ $molecule^{-1}$. No change in the shape of the $CH_3O_2$ spectrum with pressure was found from the reduced pressures (100 mbar of air and 80 mbar of He:$O_2$ = 3:1) to 1000 mbar of air, showing that $\sigma_{CH3O2}$ is almost independent of pressure. For a time averaging of 60 s the calculated CRDS *LOD* using the Allan-Werle deviation plots and $\sigma_{CH3O2}$ is around 8 × $10^9$ molecule $cm^{-3}$ using acetone/$O_2$/254 nm at all operating pressures and 6 × $10^9$ molecule $cm^{-3}$ using $CH_4/Cl_2$/black lamps at the reduced pressures.

The FAGE–CRDS intercomparison used measurements of $CH_3O_2$ under steady-state conditions (photolysis lamps on) as well as rapid decays in [$CH_3O_2$] (lamps switched off) to cover large concentration ranges: 2–26 × $10^{10}$ molecule $cm^{-3}$ at 80 mbar of He + $O_2$ mixture, 2–60 × $10^{10}$ molecule $cm^{-3}$ at 100 mbar of air and 2–30 × $10^{10}$ molecule $cm^{-3}$ at 1000 mbar of air. A good agreement between $[CH_3O_2]_{FAGE}$ and $[CH_3O_2]_{CRDS}$ was obtained under all conditions as shown by the gradient of the correlation plots: 1.03 ± 0.05 at 80 mbar He/$O_2$, 0.95 ± 0.02 at 100 mbar air and 1.09 ± 0.06 at 1000 mbar air (using an average of the sensitivity factors for the two FAGE calibration methods). The study provides a validation for the indirect FAGE method for $CH_3O_2$ measurements, in agreement with the previous FAGE validation for $HO_2$ measurements (Onel et al., 2017a).

*Data availability*. Data presented in this study are available from the authors upon request (chmlo@leeds.ac.uk and d.e.heard@leeds.ac.uk).

*Competing interests*. The authors declare that they have no conflict of interest.

**Acknowledgements**

This work has received funding from the Natural Environment Research Council (NERC grant number NE/M011208/1), the National Centre for Atmospheric Science and the European Union's Horizon 2020 research and innovation programme through

the EUROCHAMP-2020 Infrastructure Activity under grant agreement No 730997. AB thanks to NERC for a studentship awarded in the framework of the SPHERES doctoral training programme (NE/L002574/1). The authors thank Christa Fittschen for helpful discussions on the absorption cross section of $CH_3O_2$.

## References

Assaf, E., Sheps, L., Whalley, L., Heard, D., Tomas, A., Schoemaecker, C., and Fittschen, C.: The reaction between $CH_3O_2$ and OH radicals: product yields and atmospheric implications, Environmental Science & Technology, 51, 2170-2177, 10.1021/acs.est.6b06265, 2017.

Atkinson, D. B., and Spillman, J. L.: Alkyl peroxy radical kinetics measured using near infrared CW-cavity ring-down spectroscopy, J. Phys. Chem. A, 106, 8891-8902, 10.1021/jp0257597, 2002.

Atkinson, R., Baulch, D. L., Cox, R. A., Crowley, J. N., Hampson, R. F., Hynes, R. G., Jenkin, M. E., Rossi, M. J., and Troe, J.: Evaluated kinetic and photochemical data for atmospheric chemistry: Volume II - gas phase reactions of organic species, Atmos. Chem. Phys., 6, 3625-4055, 2006.

Boggs, P. T., Byrd, R. H., and Schnabel, R. B.: A stable and efficient algorithm for nonlinear orthogonal distance regression, Siam Journal on Scientific and Statistical Computing, 8, 1052-1078, 10.1137/0908085, 1987.

Cantrell, C. A., Stedman, D. H., and Wendel, G. J.: Measurement of atmospheric peroxy-radicals by chemical amplification, Anal. Chem., 56, 1496-1502, 10.1021/ac00272a065, 1984.

Cantrell, C. A., Zimmer, A., and Tyndall, G. S.: Absorption cross sections for water vapor from 183 to 193 nm (vol 24, pg 2195, 1997), Geophysical Research Letters, 24, 2687-2687, 10.1029/97gl02803, 1997.

Chung, C. Y., Cheng, C. W., Lee, Y. P., Liao, H. Y., Sharp, E. N., Rupper, P., and Miller, T. A.: Rovibronic bands of the A <-X transition of $CH_3OO$ and $CD_3OO$ detected with cavity ringdown absorption near 1.2-1.4 μm, J. Chem. Phys., 127, 10.1063/1.2747616, 2007.

Creasey, D. J., Heard, D. E., and Lee, J. D.: Absorption cross-section measurements of water vapour and oxygen at 185 nm. Implications for the calibration of field instruments to measure OH, $HO_2$ and $RO_2$ radicals, Geophysical Research Letters, 27, 1651-1654, 10.1029/1999gl011014, 2000.

Farago, E. P., Viskolcz, B., Schoemaecker, C., and Fittschen, C.: Absorption Spectrum and Absolute Absorption Cross Sections of $CH_3O_2$ Radicals and $CH_3I$ Molecules in the Wavelength Range 7473-7497 $cm^{-1}$, J. Phys. Chem. A, 117, 12802-12811, 10.1021/jp408686s, 2013.

Fittschen, C., Whalley, L. K., and Heard, D. E.: The Reaction of $CH_3O_2$ Radicals with OH Radicals: A Neglected Sink for $CH_3O_2$ in the Remote Atmosphere, Environmental Science & Technology, 48, 7700-7701, 10.1021/es502481q, 2014.

Fittschen, C.: The reaction of peroxy radicals with OH radicals, Chem.Phys.Lett., 725, 102–108, 2019.

Fuchs, H., Holland, F., and Hofzumahaus, A.: Measurement of tropospheric $RO_2$ and $HO_2$ radicals by a laser-induced fluorescence instrument, Rev. Sci. Instrum., 79, 12, 10.1063/1.2968712, 2008.

Glowacki, D. R., Goddard, A., Hemavibool, K., Malkin, T. L., Commane, R., Anderson, F., Bloss, W. J., Heard, D. E., Ingham, T., Pilling, M. J., and Seakins, P. W.: Design of and initial results from a Highly Instrumented Reactor for Atmospheric Chemistry (HIRAC), Atmospheric Chemistry and Physics, 7, 5371-5390, 2007.

Gordon, I. E., Rothman, L. S., Hill, C., Kochanov, R. V., Tan, Y., Bernath, P. F., Birk, M., Boudon, V., Campargue, A., Chance, K. V., Drouin, B. J., Flaud, J. M., Gamache, R. R., Hodges, J. T., Jacquemart, D., Perevalov, V. I., Perrin, A., Shine, K. P., Smith, M. A. H., Tennyson, J., Toon, G. C., Tran, H., Tyuterev, V. G., Barbe, A., Csaszar, A. G., Devi, V. M., Furtenbacher, T., Harrison, J. J., Hartmann, J. M., Jolly, A., Johnson, T. J., Karman, T., Kleiner, I., Kyuberis, A. A., Loos, J., Lyulin, O. M., Massie, S. T., Mikhailenko, S. N., Moazzen-Ahmadi, N., Muller, H. S. P., Naumenko, O. V., Nikitin, A. V., Polyansky, O. L., Rey, M., Rotger, M., Sharpe, S. W., Sung, K., Starikova, E., Tashkun, S. A., Vander Auwera, J., Wagner, G., Wilzewski, J., Wcislo, P., Yu, S., and Zak, E. J.: The HITRAN2016 molecular spectroscopic database, Journal of Quantitative Spectroscopy & Radiative Transfer, 203, 3-69, 10.1016/j.jqsrt.2017.06.038, 2017.

Green, T. J., Reeves, C. E., Fleming, Z. L., Brough, N., Rickard, A. R., Bandy, B. J., Monks, P. S., and Penkett, S. A.: An improved dual channel PERCA instrument for atmospheric measurements of peroxy radicals, J. Environ. Monitor., 8, 530-536, 10.1039/b514630e, 2006.

Hanke, M., Uecker, J., Reiner, T., and Arnold, F.: Atmospheric peroxy radicals: ROXMAS, a new mass-spectrometric methodology for speciated measurements of $HO_2$ and $\Sigma RO_2$ and first results, Int. J. Mass Spectrom., 213, 91-99, 10.1016/s1387-3806(01)00548-6, 2002.

Hansel, A., Scholz, W., Mentler, B., Fischer, L., and Bernd, T.: Detection of $RO_2$ radicals and other products from cyclohexene ozonolysis with $NH_4$+ and acetate chemical ionization mass spectrometry, Atmos. Environ., 186, 248-255, 10.1016/j.atmosenv.2018.04.023, 2018.

Hernandez, M. D. A., Burkert, J., Reichert, L., Stobener, D., Meyer-Arnek, J., Burrows, J. P., Dickerson, R. R., and Doddridge, B. G.: Marine boundary layer peroxy radical chemistry during the AEROSOLS99 campaign: Measurements and analysis, J. Geophys. Res.-Atmos., 106, 20833-20846, 10.1029/2001jd900113, 2001.

Huang, D. R., Chu, L. K., and Lee, Y. P.: Infrared absorption of gaseous $CH_3OO$ detected with a step-scan Fourier-transform spectrometer, J. Chem. Phys., 127, 10.1063/1.2807241, 2007.

Jenkin, M. E., Cox, R. A., Hayman, G. D., and Whyte, L. J.: Kinetic study of the reactions $CH_3O_2$ + $CH_3O_2$ and $CH_3O_2$ + $HO_2$ using molecular modulation spectroscopy, J. Chem. Soc. Faraday Trans. II, 84, 913-930, 10.1039/f29888400913, 1988.

Jokinen, T., Sipila, M., Richters, S., Kerminen, V. M., Paasonen, P., Stratmann, F., Worsnop, D., Kulmala, M., Ehn, M., Herrmann, H., and Berndt, T.: Rapid Autoxidation Forms Highly Oxidized $RO_2$ Radicals in the Atmosphere, Angew. Chem. Int. Ed., 53, 14596-14600, 10.1002/anie.201408566, 2014.

Kline, N. D., and Miller, T. A.: Observation of the A - X electronic transition of C6 - C10 peroxy radicals, Chem. Phys. Lett., 601, 149-154, 10.1016/j.cplett.2014.03.087, 2014.

Kurylo, M. J., and Wallington, T. J.: The temperature dependence of the rate constant for the gas phase disproportionation reaction of $CH_3O_2$ radicals, Chem. Phys. Lett., 138, 543-547, 10.1016/0009-2614(87)80121-5, 1987.

McAdam, K., Veyret, B., and Lesclaux, R.: UV absorption spectra of $HO_2$ and $CH_3O_2$ radicals and the kinetics of their mutual reactions ant 298 K, Chem. Phys. Lett., 133, 39-44, 10.1016/0009-2614(87)80049-0, 1987.

Miyazaki, K., Parker, A. E., Fittschen, C., Monks, P. S., and Kajii, Y.: A new technique for the selective measurement of atmospheric peroxy radical concentrations of $HO_2$ and $RO_2$ using a denuding method, Atmos. Meas. Tech., 3, 1547-1554, 10.5194/amt-3-1547-2010, 2010.

Noziere, B., and Hanson, D. R.: Speciated Monitoring of Gas-Phase Organic Peroxy Radicals by Chemical Ionization Mass Spectrometry: Cross-Reactions between $CH_3O_2$, $CH_3(CO)O_2$, $(CH_3)_3CO_2$, and c-$C_6H_{11}O$, J. Phys. Chem. A, 121, 8453-8464, 10.1021/acs.jpca.7b06456, 2017.

Noziere, B., and Vereecken, L.: Direct Observation of Aliphatic Peroxy Radical Autoxidation and Water Effects: An Experimental and Theoretical Study, Angew. Chem. Int. Ed., 58, 13976-13982, 10.1002/anie.201907981, 2019.

Onel, L., Brennan, A., Gianella, M., Ronnie, G., Aguila, A. L., Hancock, G., Whalley, L., Seakins, P. W., Ritchie, G. A. D., and Heard, D. E.: An intercomparison of $HO_2$ measurements by fluorescence assay by gas expansion and cavity ring-down spectroscopy within HIRAC (Highly Instrumented Reactor for Atmospheric Chemistry), Atmos. Meas. Tech., 10, 4877-4894, 10.5194/amt-10-4877-2017, 2017a.

Onel, L., Brennan, A., Seakins, P. W., Whalley, L., and Heard, D. E.: A new method for atmospheric detection of the $CH_3O_2$ radical, Atmos. Meas. Tech., 10, 3985-4000, 10.5194/amt-10-3985-2017, 2017b.

Orlando, J. J., and Tyndall, G. S.: Laboratory studies of organic peroxy radical chemistry: an overview with emphasis on recent issues of atmospheric significance, Chem. Soc. Rev., 41, 8213-8213, 2012.

Pushkarsky, M. B., Zalyubovsky, S. J., and Miller, T. A.: Detection and characterization of alkyl peroxy radicals using cavity ringdown spectroscopy, J. Chem. Phys., 112, 10695-10698, 10.1063/1.481705, 2000.

Sander, S. P., and Watson, R. T.: Kinetic studies of the reactions of $CH_3O_2$ with NO, $NO_2$ and $CH_3O_2$ at 298 K, J. Phys. Chem., 84, 1664-1674, 10.1021/j100450a002, 1980.

Sander, S. P., and Watson, R. T.: Temperature dependence of the self-reaction of $CH_3O_2$ radicals, J. Phys. Chem., 85, 2960-2964, 10.1021/j150620a023, 1981.

Sharp, E. N., Rupper, P., and Miller, T. A.: The structure and spectra of organic peroxy radicals, Phys. Chem. Chem. Phys., 10, 3955-3981, 10.1039/b800954f, 2008.

Simon, F. G., Schneider, W., and Moortgat, G. K.: UV absorption spectrum of the methylperoxy radical and the kinetics of its disproportionation reaction at 300 K, Int. J. Chem. Kinet., 22, 791-812, 10.1002/kin.550220802, 1990.

Sprague, M. K., Mertens, L. A., Widgren, H. N., Okumura, M., Sander, S. P., and McCoy, A. B.: Cavity Ringdown Spectroscopy of the Hydroxy Methyl Peroxy Radical, J. Phys. Chem. A, 117, 10006-10017, 10.1021/jp400390y, 2013.

Tyndall, G. S., Cox, R. A., Granier, C., Lesclaux, R., Moortgat, G. K., Pilling, M. J., Ravishankara, A. R., and Wallington, T. J.: Atmospheric chemistry of small organic peroxy radicals, J. Geophys. Res. -Atmos., 106, 12157-12182, 10.1029/2000jd900746, 2001.

Wallington, T. J., Dagaut, P., and Kurylo, M. J.: Ultraviolet absorption cross-sections and reaction kinetics and mechanisms for peroxy radicals in the gas-phase, Chem. Rev., 92, 667-710, 10.1021/cr00012a008, 1992.

Werle, P., Mucke, R., and Slemr, F.: The limits of signal averaging in atmospheric trace-gas monitoring by tunable diode-laser absorption-spectroscopy (TDLAS), Applied Physics B-Photophysics and Laser Chemistry, 57, 131-139, 10.1007/bf00425997, 1993.

Whalley, L. K., Furneaux, K. L., Goddard, A., Lee, J. D., Mahajan, A., Oetjen, H., Read, K. A., Kaaden, N., Carpenter, L. J., Lewis, A. C., Plane, J. M. C., Saltzman, E. S., Wiedensohler, A., and Heard, D. E.: The chemistry of OH and $HO_2$ radicals in the boundary layer over the tropical Atlantic Ocean, Atmos. Chem. Phys., 10, 1555-1576, 10.5194/acp-10-1555-2010, 2010.

Whalley, L. K., Edwards, P. M., Furneaux, K. L., Goddard, A., Ingham, T., Evans, M. J., Stone, D., Hopkins, J. R., Jones, C. E., Karunaharan, A., Lee, J. D., Lewis, A. C., Monks, P. S., Moller, S. J., and Heard, D. E.: Quantifying the magnitude of a missing hydroxyl radical source in a tropical rainforest, Atmos. Chem. Phys., 11, 7223-7233, 10.5194/acp-11-7223-2011, 2011.

Whalley, L. K., Blitz, M. A., Desservettaz, M., Seakins, P. W., and Heard, D. E.: Reporting the sensitivity of laser-induced fluorescence instruments used for $HO_2$ detection to an interference from $RO_2$ radicals and introducing a novel approach that enables $HO_2$ and certain $RO_2$ types to be selectively measured, Atmos. Meas. Tech., 6, 3425-3440, 10.5194/amt-6-3425-2013, 2013.

Whalley, L. K., Stone, D., Dunmore, R., Hamilton, J., Hopkins, J. R., Lee, J. D., Lewis, A. C., Williams, P., Kleffmann, J., Laufs, S., Woodward-Massey, R., and Heard, D. E.: Understanding in situ ozone production in the summertime through radical observations and modelling studies during the Clean air for London project (ClearfLo), Atmos. Chem. Phys., 18, 2547-2571, 10.5194/acp-18-2547-2018, 2018.

Winiberg, F. A. F., Smith, S. C., Bejan, I., Brumby, C. A., Ingham, T., Malkin, T. L., Orr, S. C., Heard, D. E., and Seakins, P. W.: Pressure-dependent calibration of the OH and $HO_2$ channels of a FAGE HOx instrument using the Highly Instrumented Reactor for Atmospheric Chemistry (HIRAC), Atmos. Meas. Tech., 8, 523-540, 10.5194/amt-8-523-2015, 2015.

Wood, E. C., Deming, B. L., and Kundu, S.: Ethane-Based Chemical Amplification Measurement Technique for Atmospheric Peroxy Radicals, Environ. Sci. Technol. Lett., 4, 15-19, 10.1021/acs.estlett.6b00438, 2017.

Yan, C., Kocevska, S., Krasnoperov, L.N.: Kinetics of the Reaction of $CH_3O_2$ Radicals with OH Studied over the 292-526 K Temperature Range, J. Phys. Chem. A, 120, 6111-6121, 10.1021/acs.jpca.6b04213, 2016.

Zador, J., Taatjes, C. A., and Fernandes, R. X.: Kinetics of elementary reactions in low-temperature autoignition chemistry, Prog. Energ. Combust., 37, 371-421, 10.1016/j.pecs.2010.06.006, 2011.